TRIUMF

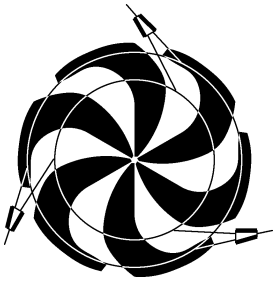

ANNUAL REPORT
SCIENTIFIC ACTIVITIES
2001

ISSN 1492-417X

CANADA'S NATIONAL LABORATORY
FOR PARTICLE AND NUCLEAR PHYSICS

OPERATED AS A JOINT VENTURE

MEMBERS:

THE UNIVERSITY OF ALBERTA
THE UNIVERSITY OF BRITISH COLUMBIA
CARLETON UNIVERSITY
SIMON FRASER UNIVERSITY
THE UNIVERSITY OF VICTORIA

ASSOCIATE MEMBERS:

THE UNIVERSITY OF MANITOBA
McMASTER UNIVERSITY
L'UNIVERSITÉ DE MONTRÉAL
QUEEN'S UNIVERSITY
THE UNIVERSITY OF REGINA
THE UNIVERSITY OF TORONTO

UNDER A CONTRIBUTION FROM THE
NATIONAL RESEARCH COUNCIL OF CANADA

OCTOBER 2002

The contributions on individual experiments in this report are outlines intended to demonstrate the extent of scientific activity at TRIUMF during the past year. The outlines are not publications and often contain preliminary results not intended, or not yet ready, for publication. Material from these reports should not be reproduced or quoted without permission from the authors.

PARTICLE PHYSICS

Experiment 497
Measurement of the flavour conserving hadronic weak interaction

(J. Birchall, S.A. Page, W.T.H. van Oers, Manitoba)

Introduction

The data analysis for the TRIUMF 221 MeV parity violation experiment, Expt. 497, was completed in early 2001 and the results have now been published [Berdoz *et al.*, Phys. Rev. Lett. **87**, 272301 (2001)]. The experiment completed data-taking in 1999 and the complete data set was analyzed during 2000 and 2001, forming the basis of an M.Sc. thesis [J. Bland, "The TRIUMF E497 parity violation experiment in the 221 MeV $\vec{p}p$ system: a complete analysis of the Feb97, Jul98 and May99 data runs" (University of Manitoba, 2001)]. Whereas previous Annual Reports have presented the results of the 1997, 1998 and 1999 runs separately, the final Expt. 497 result presented here is based on the re-analysis of all the data in a consistent way.

The experiment determines the parity violating longitudinal analyzing power, $A_z = (\sigma^+ - \sigma^-)/(\sigma^+ + \sigma^-)$, in $\vec{p}p$ elastic scattering, where σ^+ and σ^- are the scattering cross sections for positive and negative helicity. The measurements were performed in transmission geometry, with beam energy and detector geometries selected to ensure that only parity mixing in the ${}^3P_2 - {}^1D_2$ partial wave amplitude contributes to the measured parity violating asymmetry [Simonius, Can. J. Phys. **66**, 548 (1988)]. This amplitude has never been studied experimentally, and the possibility is unique to the energy regime accessible with the TRIUMF cyclotron. In the context of the weak meson exchange model [Desplanques *et al.*, Ann. Phys. (N.Y.) **124**, 449 (1980)], our measurement of A_z provides a direct determination of the weak ρ-meson-nucleon coupling constant $h_\rho^{pp} = (h_\rho^0 + h_\rho^1 + h_\rho^2/\sqrt{6})$. Precision results already obtained by the PSI group at 45 MeV [Kistryn *et al.*, Phys. Rev. Lett. **58**, 1616 (1987)] and the Bonn group at 13.6 MeV [Eversheim *et al.*, Phys. Lett. **B256**, 11 (1991); private communication (1994)] determined essentially the sum $h_\rho^{pp} + h_\omega^{pp}$. With the addition of our TRIUMF result at 221 MeV, h_ρ^{pp} and h_ω^{pp} can now be determined separately for the first time.

It is important to have experimentally determined values of the weak meson-nucleon couplings, as theoretical calculations of their values are quite uncertain and the correct values are important in the interpretation of the results of other parity violation experiments. For example, the SAMPLE (MIT Bates) result [Hasty *et al.*, Science **290**, 2117 (2000)] for the electron nucleon axial form factor is very different from calculations. The calculation requires correction for the nucleon anapole moment, a direct parity violating coupling of the photon to the nucleon. This can be computed in chiral perturbation theory, but one needs to know the weak meson-nucleon couplings.

The TRIUMF measurement will also enhance the usefulness of the $G\emptyset$ electron proton parity violation experiment at Jefferson Lab. In common with SAMPLE, correction is required for the nucleon anapole moment, which is one contribution to the effective axial form factor required to interpret the $G\emptyset$ result. Like SAMPLE, $G\emptyset$ plans to measure the axial form factor with a back angle scattering from deuterium. To the extent that the rho and omega couplings are now determined by experiment, the $G\emptyset$ axial form factor result will give an independent estimate of the weak pion-nucleon coupling, f_π^1. The most precise value of f_π^1 presently comes from the circular polarization of γ-rays from a well known parity mixed doublet in ^{18}F [Page *et al.*, Phys. Rev. **C35**, 1119 (1987); Bini *et al.*, Phys. Rev. Lett. **55**, 795 (1985)]. The experimental result is quite small compared to theoretical predictions, and Holstein [Can. J. Phys. **66**, 510 (1988)] points out that to get such a small value in a calculation, one must use current algebra quark masses which are about half the original Weinberg values. This would tend to suppress estimates in other processes, including the $\Delta I = 1/2$ rule. The $np \to d\gamma$ experiment at LANL plans a more precise measurement of f_π^1. The $G\emptyset$ experiment together with the TRIUMF pp result will provide another piece in the solution of this puzzle.

Background

This experiment was first proposed in 1985, funded in 1988, and the beam line was completed in 1994. A major effort to minimize and understand systematic error contributions was required to successfully perform an experiment with this level of precision. Following many years of effort which resulted in the reduction of both the helicity correlated beam modulations Δx_i and the sensitivities $\frac{\partial A_z}{\partial x_i}$ to these modulations, the first significant data set for Expt. 497 was acquired in February and March of 1997, with a statistical error of $\pm 0.5 \times 10^{-7}$, and most systematic errors at or below the 10^{-7} level. That result represented a major milestone for the experiment and formed the basis of the Ph.D. thesis of A.A. Hamian ["The measurement of parity violation in proton-proton scattering at 221 MeV" (University of Manitoba, 1998)]. Data-taking continued in 1998 and 1999, and the final data analysis was complete by early 2001.

Beam line and instrumentation

In addition to the measuring apparatus itself, the TRIUMF optically pumped polarized ion source (OPPIS), the cyclotron, and the transport beam lines must be considered critical components of the experimental set-up. All these components are illustrated in Fig. 1. A 5 μA transversely polarized beam is transported to the cyclotron through an approximately 50 m long injection beam line. The ion source Wien filter is tuned to produce vertical polarization at the entrance to the cyclotron. A 200 nA beam at 75–80% vertical polarization is extracted at 221 MeV. Spin precession through a pair of solenoid and dipole magnets results in delivery of a longitudinally polarized beam to the 40 cm liquid hydrogen target, which scatters 4% of the beam. Note that there are two complementary states of the spin transport, so-called "positive helicity" and "negative helicity" beam line tunes, which transport spin-up in the cyclotron into either + or − helicity at the parity apparatus. Half the data are acquired in each of these two beam line tune states, and consistency of the results in the two cases allows limits to be placed on systematic errors associated with the ion source alone, e.g. beam energy modulation, as discussed later in this report.

The custom-built parity instrumentation occupies approximately 10 m of the downstream section of beam line 4A/2 between the last quadrupole magnet and the west wall in the TRIUMF proton hall. Transverse field parallel plate ion chambers, TRIC1 and TRIC2, measure the beam current incident on and transmitted through the target. The parity violation signal is derived from the helicity-correlated analogue signal difference between the beam currents measured by the two TRICs. Upstream of the target are two polarization profile monitors (PPMs) to measure the distributions of transverse polarization $P_y(x)$ and $P_x(y)$ across the beam. Two intensity profile monitors (IPMs) measure the intensity distribution of beam current in x and y and are coupled to a pair of fast ferrite cored steering magnets (FCSMs) which lock the beam path on the optimum axis through the equipment. An additional IPM, located inside the LH_2 vacuum enclosure just upstream of the target, is used mainly for beam tuning.

Data acquisition

The spin of the optically pumped ion source is flipped 40 times per second in a pattern $(+--+-++-)$ or $(-++-+--+)$. This pattern makes

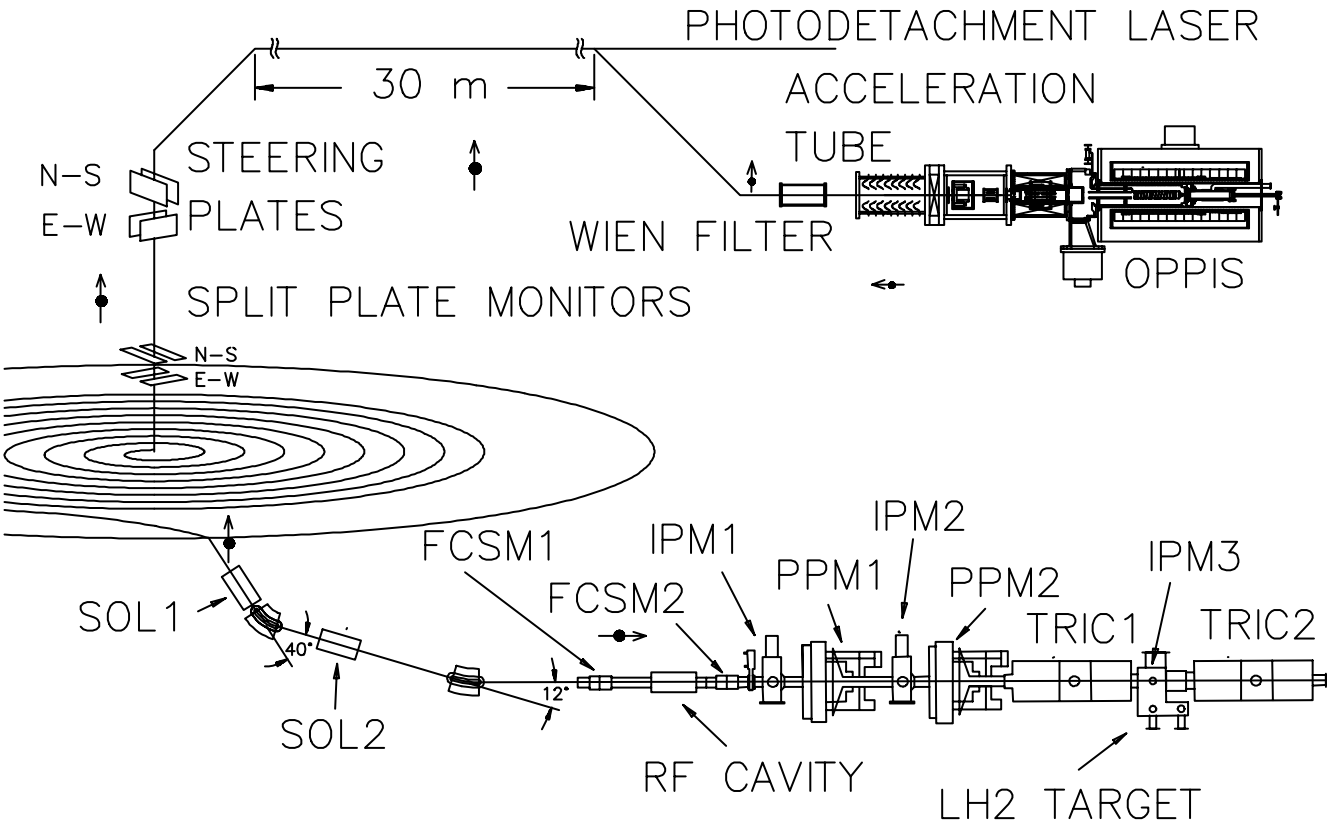

Fig. 1. General layout of TRIUMF parity experiment. (OPPIS: optically pumped polarized ion source; SOL: spin precession solenoid; FCSM: ferrite cored steering magnet; IPM: intensity profile monitor; PPM: polarization profile monitor; TRIC: transverse field ionization chamber.)

us insensitive to linear and quadratic drifts. The initial state of each 8 state (200 ms) group is also made to follow the same $(+--+-++-)$ or $(-++-+--+)$ pattern, forming a 64 state "supercycle". The initial spin state of each supercycle is chosen at random. 20% of the data is taken with all the spin flipping equipment running, but with the pumping lasers blocked with a shutter to guarantee zero polarization. Of this lasers blocked data, half is taken with an artificially enhanced intensity modulation synchronized with the spin flip in order to record our sensitivity to coherent intensity modulation.

The PPMs each have four rotating CH_2 blades, two scanning horizontally and two scanning vertically. The spin flip is synchronized with the rotation of the PPMs such that the polarization profile of the beam is measured during the first part of each spin state. An 8 state "event" hence corresponds to one full 360° rotation of the PPMs and the passage of all 8 blades through the beam. The minimum data set for which a full set of helicity correlated beam properties can be extracted is a 0.4 s "event pair", as this gives both spin states for each PPM blade. Figure 2 shows the placement of the PPM and main detector (TRIC and IPM) readout intervals during one spin state. The 6.4 ms PPM interval corresponds to a 43 mm scan centred on the beam axis. The TRIC and IPM signals are integrated over exactly 1/60 second to eliminate sensitivity to 60 Hz or harmonics of 60 Hz.

Since the 0.2 s taken for one PPM rotation is exactly 12 cycles of the 60 Hz line, one would expect a given PPM blade to always pass through the beam at the same phase of the 60 Hz line. To prevent this, we introduced a small controlled phase slip. The rate of slip is programmable but, for data-taking, was set to one complete cycle of the 60 Hz line in 18 minutes.

In addition to the regular data-taking runs, we made many dedicated control measurements to measure the sensitivity of our apparatus to various helicity correlated beam properties.

The data set

The parity data set used in our final analysis was acquired during three major data runs: February–March, 1997, July–August, 1998, and May–June, 1999. Statistics for the combined set are:

- 3.8 million event pairs
- 375 runs in positive beam line helicity
- 368 runs in negative beam line helicity
- 80 position modulation runs
- 81 size modulation runs
- 40 energy modulation runs
- 109 neutral axis scans.

The data were grouped into 23 sets, the data in each set sharing the same beam line tune. The top panel in Fig. 3 shows the data from the 23 sets after data obtained under bad running conditions had been cut (see the next section), but before corrections were made for systematic errors. The bottom panel shows the corrected data from which our final result was obtained.

Reduced data set

During data-taking, every effort was made to maintain the optimum beam conditions (quiet beam, good

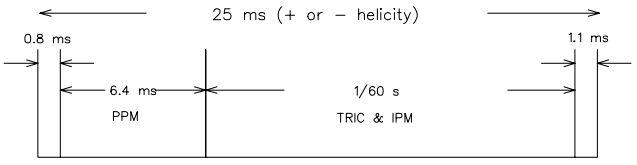

Fig. 2. The placement of detector readout intervals within one spin state. The 6.4 ms PPM interval corresponds to a 43 mm scan centred on the beam axis. The TRIC interval is 1/60 second to eliminate sensitivity to 60 Hz or harmonics of 60 Hz.

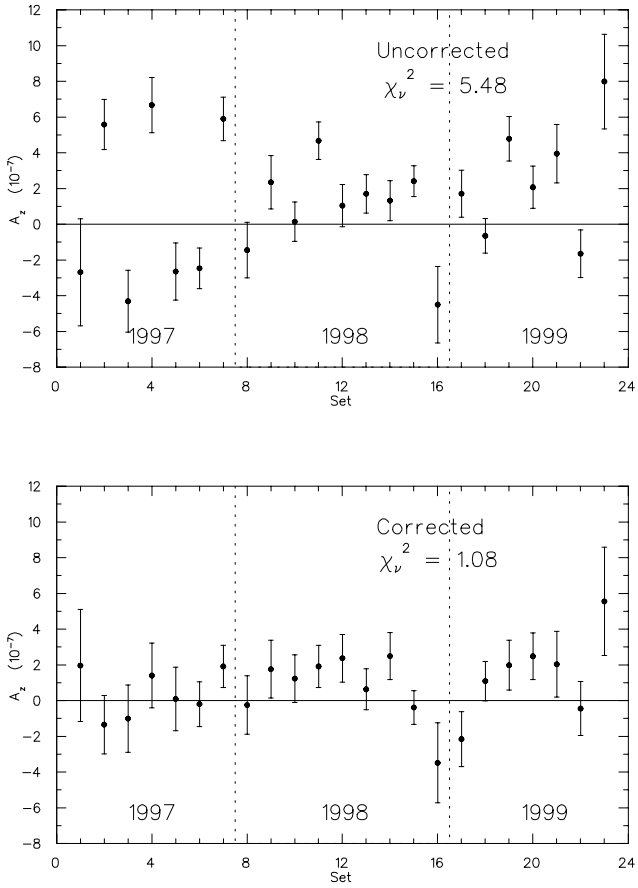

Fig. 3. Experiment 497 data before and after correction. The data are divided into 23 sets of alternating beam line tune. The top panel shows the data after beam quality cuts, but before correction for systematic error. The bottom panel shows the data after correction.

polarization, beam on axis, low transverse polarization, stable position and size, low first moments of transverse polarization, low intensity modulation), and to stop data-taking when these conditions were not met. Nevertheless, some data were taken for which conditions were not ideal. During analysis, 46 runs were first eliminated completely because the signal was anomalously noisy, indicating unstable beam conditions. The remaining data were then subjected to beam quality cuts. The cuts used are summarized in Table I. There are both "hard cuts" at a fixed value of beam parameter and "soft cuts" at $\pm 3\sigma$ from the mean value. The entire data reduction process reduced the size of the total set by 30%, but significantly improved the quality of the data sample. The χ^2_v for the 23 sets went from 11.3 per degree of freedom before the cuts were made to 5.48 after the cuts. The 23 uncorrected data on the top panel of Fig. 3 are from the reduced data set.

Table I. Summary of data reduction cuts. Except for the beam intensity, the centre of the acceptance window for each parameter is the measured centroid of that beam parameter's distribution. The hard cuts are wide enough to include at least four standard deviations.

Beam parameter	Acceptance window
Neutral axis x, y	± 0.3 mm
Average beam position	$\pm 3\sigma$ (soft)
σ_x, σ_y	± 1.0 mm
Beam skew	± 0.2 mm
Intensity	196–204 nA
Intrinsic moments	± 3.0 mm

Correction for systematic errors

The parity violating asymmetry, A_z, is determined from the helicity correlated difference between the signals in the ion chambers (TRICs) located before and after the liquid hydrogen target. Unfortunately, helicity correlated modulations of beam parameters other than helicity can, and usually do, generate a false signal of parity violation. To correct for this, helicity correlated modulations in beam intensity, size, position, transverse polarization, and first moments of transverse polarization are monitored continuously during data-taking. These unwanted modulations are then multiplied by our known sensitivities to these modulations and corrections are applied.

Coherent intensity modulation

Coherent intensity modulation is measured by the ion chamber (TRIC1) upstream of the target. The sensitivity to this modulation is measured by periods of intentional enhanced ($\sim$0.1%) intensity modulation interleaved with the main data-taking.

Coherent position modulation

Coherent position modulation is measured by two intensity profile monitors (IPMs in Fig. 1) located 1.8 m apart along the beam line. Using two IPMs permits us to measure both tilts and parallel shifts of the beam. The sensitivity to beam motion is measured in separate control measurements during which the beam position is modulated in a variety of ways using the ferrite cored steering magnets (FCSMs).

We parameterize the false analyzing power arising from helicity correlated beam position as

$$\begin{aligned}\Delta A_z = &\left(\frac{\Delta x_1 + \Delta x_2}{2}\right)(a_x x_1 + b_x x_2 + c_x) \\ &+ \left(\frac{\Delta x_1 - \Delta x_2}{2}\right)(d_x x_1 + e_x x_2 + f_x) \\ &+ \left(\frac{\Delta y_1 + \Delta y_2}{2}\right)(a_y y_1 + b_y y_2 + c_y) \\ &+ \left(\frac{\Delta y_1 - \Delta y_2}{2}\right)(d_y y_1 + e_y y_2 + f_y)\end{aligned}$$

where Δx and Δy are the horizontal and vertical helicity correlated beam motion, x and y are the beam position and the 1 and 2 subscripts refer to IPM1 and IPM2. The parameters a to f are extracted from a fit to the calibration data.

Coherent beam size modulation

Coherent beam size modulation is also measured by the two IPMs. The sensitivity to beam size is determined by control measurements in which the beam size is intentionally modulated by driving the ferrite cored steering magnets as quadrupoles.

We parameterize the false analyzing power due to beam breathing as

$$\begin{aligned}\Delta A_z = &\alpha_x \sigma_{x_1} \Delta\sigma_{x_1} + \beta_x \sigma_{x_2} \Delta\sigma_{x_2} \\ &+ \alpha_y \sigma_{y_1} \Delta\sigma_{y_1} + \beta_y \sigma_{y_2} \Delta\sigma_{y_2}\end{aligned}$$

where σ is the RMS beam size and $\Delta\sigma$ is the helicity correlated change in beam size. As with position modulation, the parameters are extracted from a fit to the calibration data. Because the beam steers somewhat when the size is modulated, correction for position modulation must be included in the fit.

Transverse polarization

Transverse polarization is measured by the two polarization profile monitors (PPMs in Fig. 1) located 1.8 m apart along the beam line. The sensitivity to transverse polarization components is measured in a series of "neutral axis scans" in which a vertically polarized beam is scanned horizontally and a horizontally polarized beam is scanned vertically. These calibration scans also determine the beam axis on which we are

insensitive to average transverse polarization components. During data-taking, the beam is held on this neutral axis by a servo system. The false parity violating signal arising from average transverse polarization is proportional to the size of the transverse component multiplied by the distance from the neutral axis – i.e. to the first moment of transverse polarization. In units of 10^{-7} per μm, the sensitivity to $\langle y\rangle\langle P_x\rangle$ is 1.9 at PPM1 and –2.5 at PPM2. The sensitivity to $\langle x\rangle\langle P_y\rangle$ is –1.5 at PPM1 and 2.0 at PPM2.

Intrinsic first moments of transverse polarization

Intrinsic first moments of transverse polarization are also measured by the PPMs. The first moments, $\langle x\rangle\langle P_y\rangle$ and $\langle y\rangle\langle P_x\rangle$, discussed in the previous section are referred to as extrinsic first moments. They arise when a beam with a net transverse polarization is displaced from the neutral axis, and can be reduced to zero by holding the beam on the neutral axis. By contrast, intrinsic moments, $\langle xP_y\rangle$ and $\langle yP_x\rangle$, result from a distribution of transverse polarization across the beam; they are not changed by moving the beam, and can be large even if the net transverse polarization is zero (for example, the polarization could be up on one side of the beam and down on the other).

Since there are no magnets after the first PPM, the first moments of transverse polarization vary linearly with position along the beam line. Furthermore, for a fixed setting of the upstream beam line magnets, the first moments at PPM1 and PPM2 tend to scale together so that, over a wide range of first moments, the ratio of first moments at PPM1 and PPM2 has a constant value. Since the neutral axis scans show that the first moment sensitivity at PPM1 is of opposite sign to, and 75% of the magnitude of, that at PPM2, it means that if the PPM2 first moment was always 75% of the PPM1 first moment, then the effective sensitivity to first moments would be zero. By adjusting the beam convergence, we attempted to achieve this magic moment ratio, but in the end the cancellation was not perfect and the residual, effective, first moment sensitivity had to be extracted from the data. This could be done either by regressing the first moment ratio from the data and using the sensitivities measured in the neutral axis scans, or by regressing the correlation of A_z with average first moment directly from the data. This latter method produced the least statistical spread and was the method used.

Energy modulation

Energy modulation cannot be measured directly at the parity apparatus. To cancel its effects, we make use of the fact that when the beam line helicity is reversed, the effects of true A_z reverse, but the effects of energy modulation do not. The 23 sets in Fig. 3 are taken with alternating beam line helicity. That the χ^2_ν is only 1.08 shows that effects from energy modulation are small. What effects are present will tend to cancel in the final average. In addition to the frequent reversals of beam line helicity, we made frequent measurements of energy modulation at the ion source and of our sensitivity to this modulation. This information was used to include the effects of uncorrected energy modulation in our error budget, as described in more detail in the next section.

Method of applying the corrections

The false A_z arising from a given coherent modulation is found by multiplying the unwanted modulation by the sensitivity to that modulation. We refer to errors from variance of the corrected A_z distribution as "statistical". The error quoted is the standard error in the mean of the A_z distribution. We refer to errors resulting from uncertainties in the sensitivities as "systematic" (even though they are statistical in nature) because an incorrect sensitivity will cause a systematic shift in the mean of the A_z distribution. There are 23 such distributions, corresponding to 23 beam line tunes of alternating helicity. Figure 3 shows the 23 corrected and uncorrected data sets and Table II summarizes the overall corrections.

To produce the corrected data the following procedure was adopted.

1. The data in each set were grouped into bundles of 10,000 event pairs per bundle.

2. Each bundle was corrected according to the observed coherent modulations (except position and size) for that bundle, giving a corrected A_z for each bundle. The variance of corrected A_z values in a set determined an error bar for that set. We call this the "statistical" error. We did not correct for position and size, because the net correction was consistent with zero and when

Table II. Corrections for systematic error. The table shows the average value of each coherent modulation, the false A_z resulting from that modulation, and the uncertainty resulting from correcting for it.

Property	Average value	$10^7\Delta A_z$
$A_z^{\rm uncorr}(10^{-7})$	1.68 ± 0.29(stat)	
$y * P_x(\mu\text{m})$	-0.1 ± 0.0	-0.01 ± 0.01
$x * P_y(\mu\text{m})$	-0.1 ± 0.0	0.01 ± 0.03
$\langle yP_x\rangle(\mu\text{m})$	1.1 ± 0.4	0.11 ± 0.01
$\langle xP_y\rangle(\mu\text{m})$	-2.1 ± 0.4	0.54 ± 0.06
$\Delta I/I$(ppm)	15 ± 1	0.19 ± 0.02
Position + size		0 ± 0.10
ΔE(meV)	7–15	0.0 ± 0.12
Total		0.84 ± 0.17(syst)
$A_z^{\rm corr}(10^{-7})$	0.84 ± 0.29(stat) ± 0.17(syst)	
χ^2_ν (23 sets)	1.08	

the corrections were applied they actually increased the residual correlations of A_z with position and size.

3. The uncertainties in the nil correction for position and size modulation were added in quadrature to each of the 23 sets. We include this in what we report in Table II as "systematic" error.

4. The errors resulting from uncertainties in the various sensitivities were added in quadrature to the corresponding data. The errors on the sensitivities are independent of what is accounted for in step 2, so it is justified to add them in quadrature to get the total error bar on each of the corrected A_z for the 23 sets. We also include this uncertainty in the "systematic" error in Table II.

5. The A_z we report is the weighted mean of the 23 data sets with a weight $1/\mathrm{err}^2$, where err is the "total" error not including energy modulation. It is this total error that is shown in the bottom panel of Fig. 3.

6. As mentioned earlier, the correction for energy modulation is tricky as we could not make a direct measurement of this in the beam line. We do have frequent measures of energy modulation at OPPIS and of dA_z/dE_{OPPIS}. These were separate control measurements taken with the pumping lasers blocked. The dA_z/dE_{OPPIS} runs were first corrected for all known systematic errors (dominated by dI/I), and we assumed that the residual false A_z was from energy modulation. The energy modulation sensitivities depend on the beam line tune, so we looked at the distribution of measured energy modulation values and dA_z/dE_{OPPIS} values for a given beam line tune and estimated a correction and a "worst case" uncertainty in the correction.

7. Corrections were calculated for energy modulation on a year by year basis. 1998 and 1999 required two corrections each, one for each beam line helicity. 1997 needed four corrections, as we had different Wien filter settings as well. Finally, all the energy modulation corrections were combined and one correction was applied to the final A_z.

8. The energy modulation correction shown in Table II is the net effect of energy modulation over the 1997, 1998 and 1999 runs. The net correction is zero. The ± 0.12 uncertainty we assign comes from the quadrature sum of the error in energy modulation plus the error in the energy modulation sensitivity. This was not included in the individual error bars for the 23 A_z numbers because we do not know the energy modulation well enough. This means the chi squared for the 23 sets is larger than it really "should" be if we knew the energy modulation error for each of the 23 sets. The fact that $\chi^2_\nu = 1.08$ without taking this into account indicates that uncorrected energy modulation effects must be small.

We know the dA_z/dE in the beam line from measurements made using an rf accelerating cavity placed upstream of IPM1 in the beam line. The result of $(2.9 \pm 0.3) \times 10^{-8}$ eV^{-1} agreed well with predictions based on variation of stopping power with energy. Based on this, the dA_z/dE_{OPPIS} we measured indicates that the cyclotron amplified dE_{OPPIS} by a factor of about 130. This is reasonable because direct measurements we made in beam line 4B indicated a factor of about 100 to 200.

Results

The overall result for the 23 sets is summarized in Table II in units of 10^{-7}. The uncorrected value of A_z is 1.68 ± 0.29(stat). We estimate that half of the uncorrected A_z comes from true parity violation and half from the various sources of systematic error as itemized in Table II. After correcting for systematic errors, we find the longitudinal analyzing power to be $A_z = 0.84 \pm 0.29(\mathrm{stat}) \pm 0.17(\mathrm{syst})$.

Conclusion

A_z in $\vec{p}p$ scattering has already attracted considerable theoretical interest, and many calculations have been made [Driscoll and Miller, Phys. Rev. **C39**, 1951 (1989); *ibid.*, **C40**, 2159 (1989); Grach and Shmatikov, Phys. Lett. **B316**, 467 (1993); Iqbal and Niskanen, Phys. Rev. **C42**, 1872 (1990); Driscoll and Meissner, Phys. Rev. **C41**, 1303 (1990)]. One of the main sources of uncertainty in these calculations is the value of the weak meson-nucleon couplings.

Figure 4 shows the limits on the weak meson-nucleon couplings h_ρ^{pp} and h_ω^{pp} imposed by the low energy results [Kistryn *et al., op. cit.*; Eversheim *et al.,*

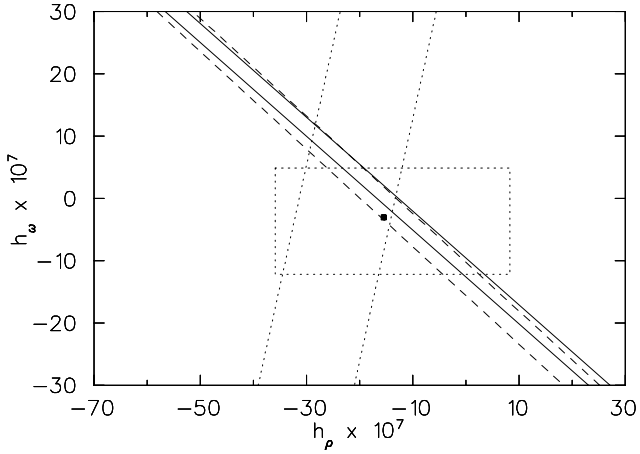

Fig. 4. Current constraints on the weak meson nucleon couplings based on the experimental data and recent calculations by Carlson and Schiavilla. The bands are the constraints imposed by different experiments (Bonn 13.6 MeV, dashed; PSI 45 MeV, solid; TRIUMF 221 MeV, dotted). The filled square and dotted rectangle are the DDH "best guess" and "reasonable range" respectively.

op. cit.; private communication (1994)], and the present TRIUMF result. The bands are based on a calculation by Carlson and Schiavilla [private communication (2001)] assuming the Argonne v_{18} (AV-18) potential [Wiringa *et al.*, Phys. Rev. **C51**, 38 (1995)], the Bonn 2000 (CD-Bonn) [Machleidt, Phys. Rev. **C63**, 24001 (2001)] strong interaction coupling constants, and including all partial waves up to $J = 8$. One sees that the TRIUMF measurement has greatly reduced the acceptable range of both h_ρ^{pp} and h_ω^{pp} over what was the case when only the low energy measurements were available.

Better values for the weak meson-nucleon coupling will be valuable in sharpening the theoretical interpretation of upcoming ep parity violation experiments such as $G\emptyset$ at Jefferson Lab. By combining the results of several seemingly disparate experiments one can finally hope to get a coherent picture of NN parity violation and in turn details of the quark content of the proton itself.

Experiment 614
TWIST – the TRIUMF weak interaction symmetry test
(N.L. Rodning, Alberta)

While the standard model has been rather successful in describing and predicting diverse phenomena, it is widely regarded as an approximation to a deeper, more fundamental theory. Recent work has renewed excitement in the search for clues to that deeper theory. In particular, the evidence for neutrino oscillations and a possible deviation in (g-2) for the muon have sparked recent interest.

The TWIST experiment is designed to study the spectrum of positrons from μ^+ decay with a final precision of 0.01%. This will allow the extraction of the Michel parameters which characterize the spectrum at a precision ranging from approximately 10 to 30 times better than existing work. Work at this precision provides significant sensitivity to possible failures of the standard model.

The TWIST spectrometer

The TWIST spectrometer is shown in Fig. 5. The basic elements of the spectrometer include 44 precision planar drift chambers and 12 planar proportional chambers. The drift chambers are used to reconstruct the trajectory of the decay e^+ while the proportional chambers are used to accurately determine the decay time. The planar geometry means that the material seen by the decay particles scales with $1\cos(\theta)$, ensuring reliable corrections for scattering and energy loss.

A polarized muon beam enters from the left and triggers the experiment by leaving a signal in a thin plastic scintillator (not shown). The muon is stopped

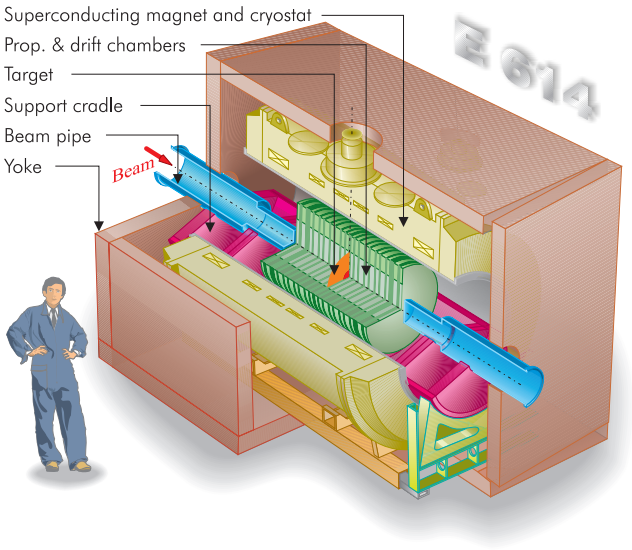

Fig. 5. The TWIST spectrometer.

at the centre of the spectrometer in a thin mylar foil. In the end, metallic targets will be used due to their decreased effect on the muon polarization.

The entire detector is in a highly uniform 2 T magnetic field, provided by a 1 m bore superconducting solenoid and shaped by a 30 ton iron return yoke.

Muons are brought into the spectrometer typically one at a time. Activity in the drift and proportional chambers is recorded for 6 μs before, and for 10 μs after, the trigger signal.

The entire spectrometer has been built and was studied during an initial commissioning run in November/December, 2001. Fabrication of spare detector planes continues.

Hardware performance

The TWIST spectrometer appears to be performing at or beyond expectations. Critical considerations include

- Average geometrical uniformity
- Single cell efficiencies
- Tracking resolution
- Field uniformity
- Depolarization (required for $P_\mu\xi$).

Average geometrical uniformity

The wires are strung across precision glass rulers at a spacing of 4 mm for the drift planes and 2 mm for the proportional chamber planes. The position of each wire is subsequently mapped using a digital microscope travelling on a precision ruler. For the drift planes, the average spacing matches the design goal to an accuracy of approximately 0.06 μm, roughly 30 times better than the design tolerance. Individual wire

positions scatter from their nominal positions with a standard deviation of approximately 3 μm, or approximately 7 times better than the design specification.

Single cell efficiency

A preliminary measurement of the efficiency of the cells yields a value of approximately 99.8% for minimally ionizing particles. The helical tracks of the decay positrons typically involve a large number of hits so that each track is heavily overdetermined and therefore hardware inefficiency is not expected to introduce any tracking ambiguity.

Tracking resolution

The determination of the tracking resolution requires that a large number of calibrations be completed and iterated upon. For example, the determination of the decay time is required for the calculation of the drift time. The wires have been strung within the detector planes with high precision, but plane-to-plane variations in position are determined by tracking particles through the detector with zero field. Preliminary values of the calibration parameters provide tracking resolution better than the design specification of 100 μm.

Field uniformity

The magnet cryostat was opened in the summer after evidence indicated that the coils might be moving within the cryostat. Any movement at the millimetre level can lead to large axial forces which increase with additional movement. The cause turned out to be missing structural elements. The magnet was repaired and commissioned to full field in September. The magnet was then used at full field during the November/December beam period, and is scheduled for mapping during March/April, 2002. We anticipate mapping the magnet to a precision of 1 G.

Depolarization

A study of the M13 surface muon beam properties was the subject of Robert MacDonald's Master's thesis [University of Alberta, 2001]. The surface muon beam has a polarization of unity if the standard model is valid. Depolarization of the beam can arise from multiple scattering in 1AT1 (the pion production target), from slit edge scattering, and from effects of the beam emittance as the beam crosses the magnet's fringe field. The effects of scattering are not expected to be a problem, but the simulations will require validation using several data sets of 10^9 events each. The effects of the beam emittance will be studied during the coming year or more. We are planning to build a time expansion chamber to measure the beam characteristics with minimal disturbance to the beam.

Experiment 761
Measurement of parity violation in *pp* scattering at 221 MeV

(J. Birchall, W.T.H. van Oers, Manitoba)

Experiment 761 is a continuation of Expt. 497 to measure the parity violating longitudinal analyzing power, A_z, in *pp* scattering at 221 MeV. The aim of the experiment is to further reduce the statistical and systematic uncertainties of A_z so that, when taken together with results from low energy, tight constraints can be placed on the weak meson-nucleon coupling constants h_ρ^{pp} and h_ω^{pp}. Accurate knowledge of these coupling constants is needed, not only to test new calculations of them, but also as input for the analysis of a number of other experiments. For example, the SAMPLE experiment at MIT Bates and $G\emptyset$ at Jefferson Lab both need to calculate a correction for the nucleon anapole moment, which represents a parity violating interaction of the photon with a nucleon. Precise knowledge of the weak meson-nucleon coupling constants is needed to perform these calculations. Further details are to be found in the report on Expt. 497 in this Annual Report.

In the past year progress has been made on a number of fronts: the establishment of an enlarged collaboration containing most of the world's experts in performing this type of experiment, refining the aims of the experiment, and improvements to the optically pumped polarized ion source.

Expanded parity collaboration, updated goal for Expt. 761

Funds were received from NSERC's International Opportunity Fund to explore the possibility of establishing a wider collaboration. To this end a workshop was held at the University of Bonn, November 8–9, 2001, at which Expt. 761 and other possible parity violation experiments were discussed. Attendees included lead members of the collaborations that made the very precise measurements of A_z at low energy at Bonn and at PSI, and of the measurement at LANL. Present were experimenters from the universities of Bonn, Erlangen and Cologne, from Forschungszentrum Jülich, LANL, the Institute for Nuclear Research in Moscow, ETH Zürich, from TRIUMF and the University of Manitoba. Discussion was animated and very positive and led to a significant revision of the aims of Expt 761.

It was universally agreed that the goal for Expt. 761 had been too conservative and that we should aim for a combined statistical and systematic error on A_z reduced by a factor of two to 0.1×10^{-7}. Figure 6 shows the constraints placed on the h_ρ^{pp} and h_ω^{pp} by Expts. 497/761 and the low energy measurements marked "Bonn 13.6 MeV" and "PSI 45 MeV". The "Expt. 497"

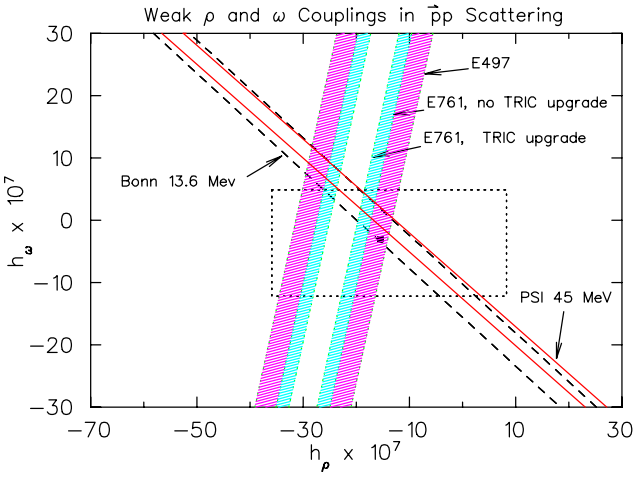

Fig. 6. Constraints on h_ρ^{pp} and h_ω^{pp} from pp scattering experiments at low energy and at 221 MeV at TRIUMF.

band shows the present constraint from Expt. 497 data alone. "Expt. 761, no TRIC upgrade" shows the original goal for Expt. 761 running at 200 nA as in Expt. 497. "Expt. 761, TRIC upgrade" shows the constraint from the updated Expt. 761 following discussions in Bonn. It is seen that the revised Expt. 761 will place a constraint on h_ρ^{pp} and h_ω^{pp} that is of comparable quality to that from the low energy measurements.

The updated goal for Expt. 761 requires a factor of four increase in data. This can be achieved by increasing beam current from 200 to 500 nA and decreasing the non-data-taking overhead. Increasing beam current will necessitate a redesign of the ionization chambers, that at present operate optimally at 200 nA, to improve noise and stability. Changes to the ion chambers include redesign of the corona shields and replacement of the sharp-edged field-shaping electrodes with a smaller number of cylindrical rods to enable the chambers to operate at their designed 20 kV in place of the 8–10 kV used in Expt. 497.

Table III shows contributions to the uncertainties in A_z from Expt. 497 and the original and updated Expt. 761. Values marked with an asterisk are conservative. They assume no reduction in systematic errors from

Table III. Contributions to uncertainties in A_z in units of 10^{-7}.

	E497		E761	E761
	200 nA		200 nA	500 nA
$A_z^{\rm uncorr}$ (stat)	1.68	±0.29	±0.20	±0.10
Ext. moments	0	±0.03	0	0
Int. moments	0.65	±0.06	0	0
$\Delta I/I$	0.19	±0.02	±0.02*	±0.01*
ΔE	0	±0.12	±0.09*	±0.04*
Position + size	0	±0.10	±0.07*	±0.03*
$A_z^{\rm corr}$	0.84	±0.34	±0.23	±0.11*

improvements made to the ion source which should significantly reduce modulations of beam properties on spin flip. The last column assumes 130 days of running at 500 nA with a reduction of data-taking overhead from a factor of five to a factor of three. Additional time will be required to commission the upgraded ion chambers and the fully-instrumented current-mode polarimeters.

Upgrades to the optically pumped ion source

Slight differences in beam properties from OPPIS on spin flip translate into changes in beam energy and current extracted from the cyclotron, which generate false parity signals. A number of upgrades have been made to OPPIS to increase current and eliminate troublesome changes of beam properties on spin flip.

New sodium ionizer

The new ionizer cell has a sodium jet, which is better at confining the sodium vapour than the old design. This means that the apertures can be made larger, thus preventing secondary electron emission, and the cell can be biased to –15 kV. The advantage of biasing the cell is that the H^- beam is accelerated as it leaves the cell, which will suppress changes of beam properties on spin flip. In addition, the reduced beam emittance at the higher beam energy will improve matching into the injection beam line to the cyclotron, and should increase the available current by a factor of 2 or 3. This would allow the source to be run at the same time as ISAC, without the bunchers which cause large beam modulations. Independent of ISAC, the source can be run in a lower current mode, with better optical pumping and polarization saturation of the rubidium vapour and therefore decreased current modulation.

New microwave generator power supply

The old power supply had considerable downtime in the last two parity runs. At RHIC a new power supply was built by Russian engineers that produces a much more stable voltage, resulting in reduced intensity fluctuations. Unlike the old supply, it also meets the warranty requirements for the new microwave tubes for the ECR dissociator.

Lasers

As the source of all helicity-correlated modulations, the lasers are critical to the experiment. OPPIS has had one titanium sapphire (TiS) probe laser to measure polarization and two TiS lasers for optical pumping of rubidium vapour, one of which is shared with the β-NMR set-up. It is planned to replace the present two standing-wave TiS optical pumping lasers with a single 6 W TiS ring laser. The TiS ring laser operates in travelling wave mode without standing waves and will exhibit less spatial mode change on spin flip. A double

etalon system with two counter-rotating etalons will further reduce spatial changes, and hence further reduce changes of beam properties on spin flip.

The ATLAS experiment at the LHC

(C. Oram, TRIUMF)

As described in detail in the 1996 Annual Report, ATLAS is building a general purpose *pp* detector which is designed to exploit the full discovery potential of the Large Hadron Collider (LHC) at CERN. The TRIUMF group is responsible for the engineering of the hadronic endcap calorimeter (HEC), and the feedthroughs for the endcap cryostat. For the HEC, this year has seen the continuation of module production and the final stages of the manufacture of the wheel assembly equipment. This year the TRIUMF HEC group has had two visitors from China as part of its close collaboration with a Chinese group. This group is a three university cluster of Nanjing University, USTC Hefei, and Shangdong University.

Physics goals

The present theoretical understanding of elementary particles is in the context of the standard model. The standard model is a remarkably successful model, providing predictions which have been consistently confirmed by experiment for over two decades. Its agreement with experimental results, to enormous accuracy in some cases, makes it the most accurately verified model in science. Of the many elementary particles contained in the standard model, only the Higgs remains to be discovered. The central goal of ATLAS is the search for the Higgs particle.

There are good theoretical reasons to believe that the discovery of the Higgs will at least contain hints of, and more likely direct evidence of, what lies beyond the standard model. If the Higgs is composite, its existence requires as yet unknown ultra-strong forces. If it is elementary, it would be the only spinless particle to be discovered so far. There is a theoretical "naturalness" problem for the masses of spinless particles. In the standard model, which is a highly nonlinear dynamical system, the elementary particles tend to take on the heaviest of all possible mass scales which in such a model are at inaccessible energies and inconsistent with other requirements of the model. All other particles discovered thus far have natural mechanisms, such as gauge and chiral symmetries, for protecting their masses so that they can lie in the observable range. For the Higgs particle, there is no such symmetry in the present model. The only theoretical scenarios which leave the Higgs particle light enough to observe are hypothetical ones, either technicolour or supersymmetry, both radical departures from the present structure of the standard model. If Higgs is seen at LHC, one of these scenarios should be seen at the same time.

Particle theory has progressed enormously over the last few decades with many appealing scenarios for physics beyond the standard model. The most likely of these is supersymmetry and the boldest of these is superstring theory. These theories are intimately related and are both radical ideas which promise a new conceptual framework for understanding elementary particles. Though far from being complete theories so far, there are superstring models which resemble the standard model in their low energy limit. These models have a great appeal as they contain a unification of fundamental forces which includes gravity. They have already had substantial impact on gravitational physics where, for example, in addition to the long sought reconciliation of gravity with quantum mechanics, they have been used to derive a fundamental understanding of black hole thermodynamics. Superstring theory is still in its infancy, but progress has been dramatic and the promise of great things to come has captured the imagination of a substantial fraction of the world's theoretical particle physicists.

The present theoretical view is that the conventional grand unification of the strong, weak and electromagnetic forces can only work in the supersymmetric extension of the standard model. In that model, the grand unified energy scale is only two decades below the Planck scale, the ultimate energy where spacetime itself has quantum fluctuations. It is not out of the realm of imagination that, at energy scales where supersymmetry would be observed, evidence for an ultimate theory of everything, at least everything that can exist once spacetime is formed, is within human grasp.

Experiments at the LHC, where the ATLAS detector will take data, will probe the energy region where the Higgs particle, possibly supersymmetry, or other structures will be visible. This will be the first experimental probe of an energy region where fundamentally new physics is expected to occur in many years. There is every reason to believe that the results will be among the most dramatic ever.

Basic ATLAS design considerations

The most prominent issue for the LHC is the quest for the origin of the spontaneous symmetry-breaking mechanism in the electroweak sector of the standard model (SM). This is related to one of the most fundamental questions of physics: What is the origin of the different particle masses? New direct experimental insight is required to answer this question.

One of the possible manifestations of the spontaneous symmetry-breaking mechanism could be the existence of a SM Higgs boson (H), or of a family of Higgs particles ($H^{\pm}$, h, H and A) when considering the min-

imal supersymmetric extension of the standard model (MSSM). The Higgs search is therefore used as a first benchmark for the detector optimization. For the SM Higgs, the detector has to be sensitive to the following processes ($\ell = e$ or μ) in order to cover the full mass range above the discovery limit set by the final LEP operation in the fall of 2000 (see Fig. 7):

$H \to b\bar{b}$ from WH, ZH and $t\bar{t}H$ using a $\ell^{\pm}$ and b-tagging,
mass range $80 < m_H < 100$ GeV;

$H \to \gamma\gamma$
mass range $90 < m_H < 150$ GeV;

$H \to WW^* \to \ell^{\pm}\nu\ell^{\pm}\nu$
mass range $150 < m_H < 200$ GeV;

$H \to ZZ^* \to 4\ell^{\pm}$
mass range 130 GeV $< m_H < 2m_Z$;

$H \to ZZ \to 4\ell^{\pm}, 2l^{\pm} + 2\nu$
mass range $m_H > 2m_Z$;

$H \to WW, ZZ \to l^{\pm}\nu + 2$ jets, $2\ell^{\pm} + 2$ jets
from WW, ZZ fusion using tagging of forward jets for m_H up to about 1 TeV.

In addition to signatures similar to these, the MSSM Higgs searches also require sensitivity to processes such as:

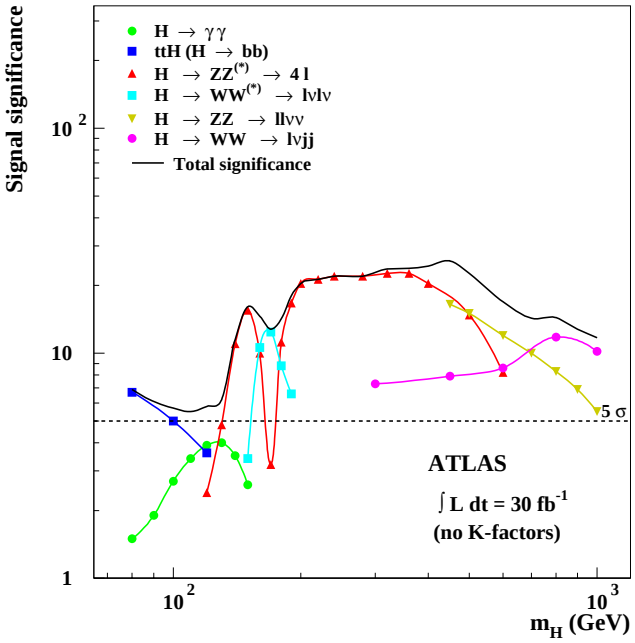

Fig. 7. Expected significance in ATLAS of the standard model Higgs boson signal, as a function of the Higgs mass, for an integrated luminosity of 10^5 pb^{-1} for several decay channels.

$A \to \tau^+\tau^-$ $\to e\mu + \nu$'s
$\to \ell^{\pm}$ + hadrons + ν's;
$H^{\pm}$ $\to \tau^{\pm}\nu$ from $t\bar{t}$ $\to H^{\pm}W^{\mp}b\bar{b}$ and using $\ell^{\pm}$ tag and b-tagging
$\to$ 2 jets.

The observable cross sections for most of these processes are small over a large part of the mass range to be explored at the LHC. Hence it is important to operate at high luminosity, and to maximize the detectable rates above backgrounds by high-resolution measurements of electrons, photons, and muons.

Canada's participation in ATLAS

The Canadian group consists of 29 grant eligible physicists from TRIUMF, University of Alberta, Carleton University, UBC, IPP, Université de Montréal, UQAM, Simon Fraser University, University of Toronto, University of Victoria, and York University. We are strongly involved in three construction projects centred around detecting hadrons in the endcap region: the hadronic endcap project, the hadronic portion of the forward calorimeter project, and the pipeline electronics for calorimetry. In addition we are committed as part of our common project contribution to providing the feedthroughs for the two endcap cryostats. TRIUMF is directly involved in all these projects, and in the trigger and physics simulations.

The hadronic endcap project

The hadronic endcap calorimeter (HEC) is a liquid argon sampling calorimeter with copper absorbers [ATLAS Collab., ATLAS Liquid Argon Technical Design Report, December 15 (1996)]. A concise overview of this design was provided in the 1996 TRIUMF Annual Report. An artist's impression of a module can be seen in Fig. 8.

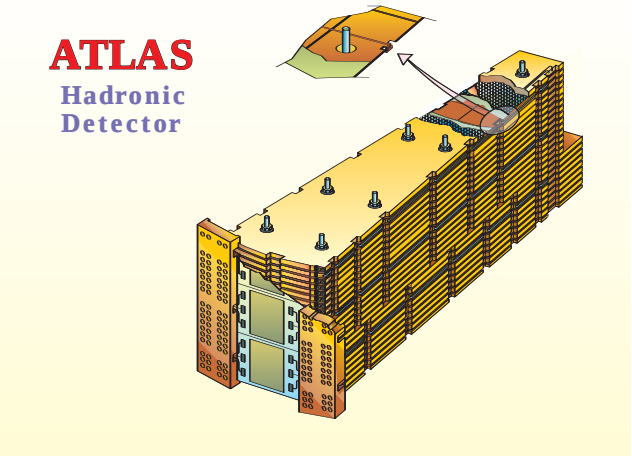

Fig. 8. Artist's impression of a hadronic endcap module.

Hadronic endcap module production

This year the major scheduled milestone was the series module production of one complete endcap, consisting of 2 wheels. By the end of the year the TRIUMF group was 70% complete on module production. The copper machining facility at the University of Alberta completed all machining for the Canadian contribution during the summer of 2001, and then moved on to helping the European group finish their allocation in a timely manner.

Test beam measurements of the hadronic endcap modules

Two test beam periods on the CERN H6 beam line this year have tested the performance of the series production modules of the calorimeter. The H6 beam line provides beams from 20 to 180 GeV. Analysis of the data shows the response is the same as in previous years. This data-taking successfully completes the quality control tests of an eighth of our series modules. A NIM paper has been submitted detailing the stand-alone behaviour of the calorimeter with pions, muons, and electrons. These measurements have been discussed in previous TRIUMF Annual Reports so we omit any details here and refer those interested to the NIM paper. To be ready for ATLAS, further test beam measurements with the other calorimeters in the endcap region "EM EndCap" and "Forward" are planned in the coming years.

In ATLAS the operating parameters for the liquid argon calorimeter will differ from those used and accessible in test beam measurements. The ATLAS system is based on the use of subcooled liquid argon, and the pressure is defined by the hydrostatic pressure at a given position in the endcap cryostat and the operating over pressure at the top surface of the liquid argon. To transfer calibration constants and signal shape parameters from the test beam results to ATLAS, the pressure and temperature effects have to be well understood. These dependencies have been studied during the summer of 2001 in beam tests at CERN using 119 GeV electrons.

To understand the temperature variation, the electron's signal was measured at a variety of argon temperatures and beam impact positions in the calorimeter. The temperature range accessible in the test beam cryostat was about 3 K. Figure 9 shows the dependence of the electron drift time, across the 1.8 mm readout gaps, on the liquid argon temperature. The data points are the measurements of the beam test. Also shown is the expected temperature range in ATLAS and the linear extrapolation of the data. Figure 10 shows the dependence of the primary signal current on the liquid argon temperature. Again the data are shown with a linear extrapolation into the ATLAS operating region. In

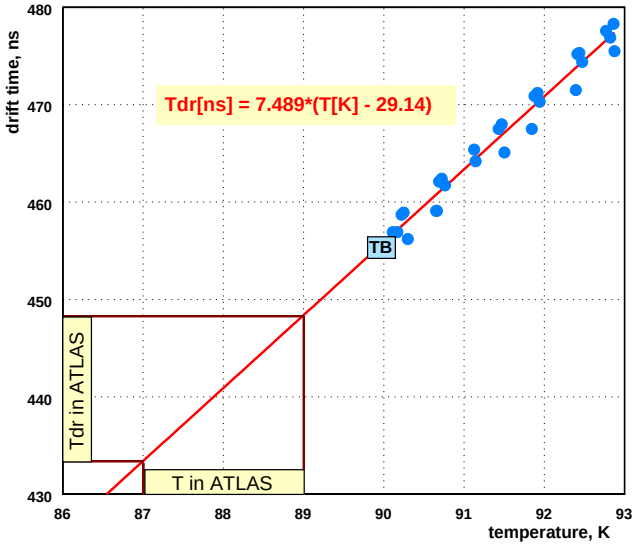

Fig. 9. Temperature dependence of drift time.

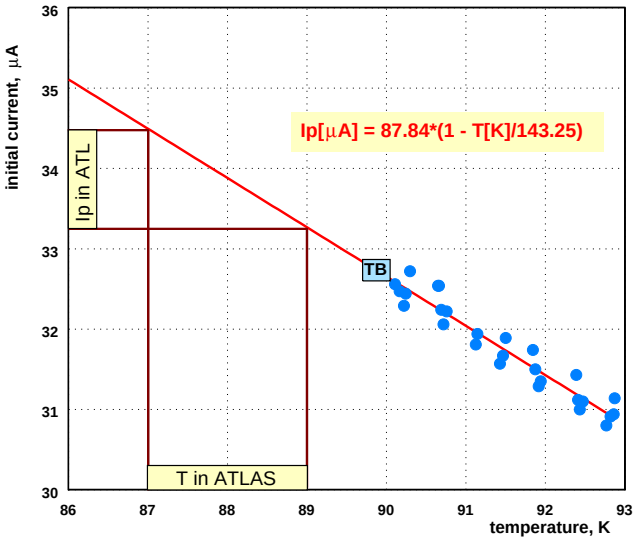

Fig. 10. Temperature dependence of primary current signal.

ATLAS we thus expect about 3.6% larger signals than in the beam test.

Preparations for wheel assembly at CERN

32 modules of the HEC form a wheel. There are two wheels at each end of ATLAS, so we must construct 128 modules into four wheels. The equipment to undertake this is a Canadian responsibility. These four wheels and the two wheels of the EM calorimeter, which go in the same calorimeter, are assembled in the horizontal orientation. Hence each wheel, which weighs about 90 tonnes, must be taken from its assembly table, rotated to the vertical and moved to the cryostat. This translation and rotation of equipment is a Canadian responsibility. The engineering was undertaken by

Fig. 11. Wheel assembly tooling on truck outside manufacturing plant in Ontario.

Fig. 12. Wheel rotation tooling inside manufacturing plant in Ontario.

Fig. 13. Wheel rotation tooling and assembly table inside manufacturing plant in Ontario.

a collaboration between Alberta and TRIUMF personnel. The production of the equipment was in Canadian industry. Figure 11 shows a portion of this equipment being transported between manufacturer sites in Ontario in late fall. Figures 12 and 13 show views of some of the equipment assembled at the manufacturing site.

The ATLAS endcap signal feedthroughs

(M. Lefebvre, Victoria)

The TRIUMF group is responsible for the engineering of the HEC and contributes to the production of high density cryogenic signal feedthroughs for both endcap cryostats. The feedthroughs are critical to the success of ATLAS. They are being built and tested at the University of Victoria by TRIUMF and Victoria staff. The endcap signal feedthroughs are currently scheduled to be installed on the two endcap cryostats during two periods starting approximately March, 2002 and October, 2002. At the end of 2001, approximately 1.5 months remained until the completion of this 7 year project. As this is the first time the endcap signal feedthrough project is covered in significant details in a TRIUMF Annual Report, the most important aspects of the project are reviewed.

Responsibilities, management and reviews

The ATLAS collaboration has determined that some components of the detector can be regarded as contributions in kind to the Common Fund; these are known as Common Fund Projects. The endcap signal feedthroughs are part of the Canadian group contribution to the Common Fund. The Canadian group is responsible for the assembly, testing, and commissioning of the ATLAS endcap signal feedthroughs, as well as participation in their installation on the cryostats. The design of the feedthrough was made in collaboration with the Brookhaven National Laboratory (BNL), which is responsible for the production of the barrel cryostat signal feedthroughs.

A Canadian involvement in the endcap signal feedthroughs was already proposed in 1995. From the $12.2 M Major Installation Grant awarded to ATLAS in the 1997–98 competition, a total of $4.28 M is earmarked for the endcap signal feedthrough project. Considerable effort has been spent developing the management tools needed for successful completion of the project. Documents describing in detail the feedthrough design, the assembly procedures, the test procedures, the procurement plan, the quality assurance plan, and the material traceability are available. The administrative structure needed for duty exemption for goods for re-export has been set up in Victoria.

ATLAS reviews of the feedthrough project were held at BNL on June 12–13, 1997, and at CERN

on October 13–15, 1997, and October 2, 1998. The feedthrough Production Readiness Review (PRR) took place at CERN on January 29, 1999, where the green light was given for the procurement of the glass technology pin carriers. Status reports were presented at three NSERC ATLAS Reviews (TRIUMF, January 9, 2000, October 19, 2000 and December 14, 2001).

Overview of the project

The ATLAS liquid argon calorimetry is composed of a barrel section and two endcap sections. Each endcap cryostat contains an electromagnetic calorimeter, two wheels of one HEC, and a forward calorimeter. The calorimeter signal and calibration lines are routed to the outside of each endcap cryostat via 25 feedthrough assemblies arranged approximately equally spaced in azimuth. The low voltage needed to operate the endcap hadronic calorimeter preamplifiers, which are located in the cold region, are also supplied via the signal feedthroughs as well as various monitoring lines.

The specifications that drove the technical design of the feedthrough assembly are quite complex. They involve geometrical and space constraints in the cryostat design, physical limitations on the space which is allocated to the feedthroughs, signal transmission quality, vacuum integrity, heat loss considerations, access possibilities, installation, reliability, and cost issues.

The design is based on gold plated conductive pins insulated and sealed by glass inserts in a stainless steel carrier. The carriers are then welded into the cold and ambient (temperature) flanges. A total of 1920 signal and calibration lines per feedthrough assembly is required in the chosen design. The ambient and cold flanges are connected by a bellows to isolate the feedthrough vacuum from the cryostat inter-vessel vacuum. The cold flange is attached to a transition piece, known as a funnel, which is welded to the cryostat via a bi-metallic joint. The electrical signals are brought from the calorimeter to the cold flange by coaxial kapton cables; these are called pigtail cables. Cables located in the vacuum between the cold and the ambient flange, i.e. inside the bellows, carry the signals through the cryostat wall; these are called vacuum cables. For each endcap, four feedthrough assemblies also carry the low voltage for the HEC preamplifiers. Figure 14 shows an overview drawing of one endcap signal feedthrough.

Project set-up

The project set-up comprises the hardware and software required for the production of the feedthrough assemblies. The most important items are the leak test station, the electric test station, and the assembly jigs.

Leak test station

The selected glass technology for the signal feedthrough is mature and has shown good results in

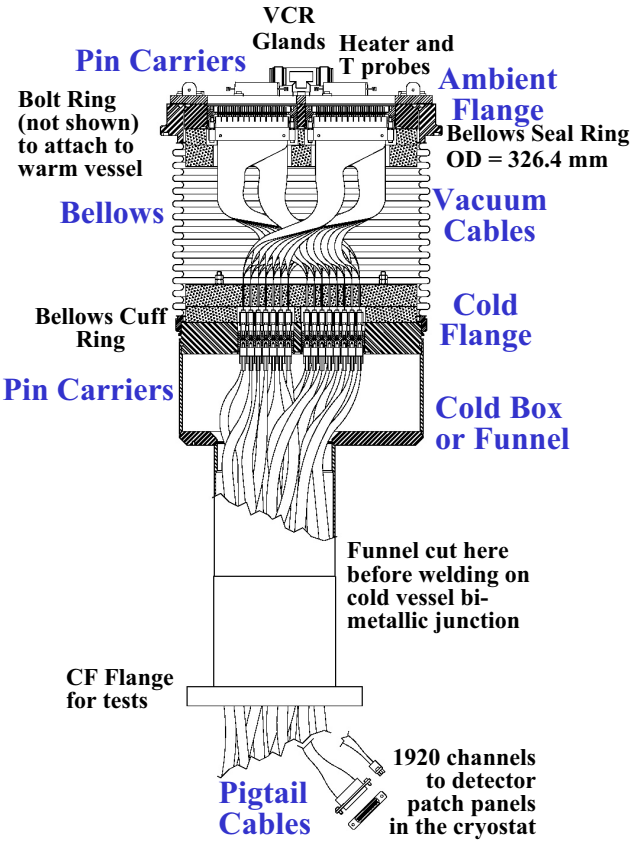

Fig. 14. Overview drawing of one endcap signal feedthrough, identifying its most important components.

applications that require high reliability under extreme temperature and pressure conditions. Still, the application considered here is pushing technology to its limits in order to reach the required density. The failure rate that we can tolerate is essentially zero over 20 years of operation. Since access to the various feedthrough assembly parts will be limited, a detailed and comprehensive testing procedure is vital.

Following the experience acquired at BNL, we have designed and assembled a leak test station that allows warm and cold leak tests to be performed in a controlled way. A precision of 1×10^{-9} atm.cc/s is required and has been achieved. The station is based on a helium leak checker, a residual gas analyzer and various pressure and temperature probes that service a warm test station for feedthrough assembly components, and a cold test station for full assemblies. Measurements are read by a PC based LabView DAQ system developed in Victoria. This test station is fully operational.

Electric test station

The feedthrough cables are used to carry analogue signals from the cryostats to the outside world, as well as calibration signals into the cryostats. Because of the fast shaping, the signal integrity is a major concern.

The grounding and shielding must be of good quality to avoid signal deterioration.

We have developed the electric test station needed to certify the electrical integrity of the signal feedthroughs. This station provides automated measurements of cable resistance, impedance and crosstalk. It uses, among other components, a network analyzer for detailed transient tests, a purpose built channel scanner developed in Orsay and assembled at UBC, and a purpose built channel multiplexer developed at UBC. Measurements are read by a PC based LabView DAQ system developed in Victoria. The instrumentation for testing the low voltage distribution for the HEC feedthrough units has also been developed. This test station is fully operational.

Assembly jigs

Each feedthrough assembly is too heavy to be handled manually. Assembly jigs and related hoists have been developed and built to allow the various phases of the assembly to be performed. In particular, the proper relative orientation of the flanges is ensured by the jigs' design.

Prototyping

Since 1997, our group has produced a full scale model, and purchased or produced prototypes of the various components of a feedthrough assembly. These were vital to the finalization of the design, the assembly procedures, including the welds, and the choice of suppliers. We have then used prototype parts to construct a feedthrough assembly with a dismountable flange-bellows interface. This prototype, which can easily be reconfigured, has been extensively used for the study of convective thermal loss and the study of leak and electric test procedures. We have also constructed a mechanical prototype to allow the cryostat team to perform various installation tests.

Final design

Contributions to the design of feedthrough assembly components through finite element analyses (FEA) were initiated early in 1996. These analyses, performed by Terry Hodges (TRIUMF), include detailed FEA of the mechanical stresses and deformation for the cold and ambient flanges, equipped with pin carriers, for various design options. Further mechanical stress analyses were performed for the funnel and the bi-metallic joint. These led to design guidelines suitable for both the barrel and endcap feedthrough assemblies. FEA studies of the flange temperature validate the plan to heat the ambient flange via resistors, and prescribe a maximum cooling rate for a safe cold testing of the equipped flanges. A detailed design of the ambient flange heater plate system has been finalized in 2000.

Procurement of components

Vacuum cables

The development of signal vacuum cables in Canada was successfully completed in 1998. Prototype assemblies have been designed and constructed in Canada in collaboration with CRPP and STC. These cable assemblies have been sent for tests to the BNL and LAL/Orsay laboratories. One cable has been irradiated in Grenoble in July, 1998 and successfully inspected and tested in Victoria. The performance of these prototypes was very encouraging. A series preproduction of 100 cables was launched at STC late in 1998, and received in the spring of 1999. These cables were extensively tested and found to perform as required. Meanwhile the BNL team has chosen FCI-BERG as the supplier of the barrel feedthrough vacuum cables. Following a Request For Quote sent to both FCI-BERG and STC for the endcap feedthrough signal vacuum cables, our group also opted for FCI-BERG as suppliers. We have now received all 1750 vacuum cables.

Special vacuum cables have been developed for the distribution of the HEC low voltage. Detailed tests with a complete low voltage HEC chain have been performed in Victoria in October, 1999. We have ordered and received all 40 HEC low voltage vacuum cables from Axon.

Pigtail cables

The development of the pigtail cables was part of a larger effort to develop signal and calibration cables for the whole of the LAr readout chain. The pigtail cables for the endcap signal feedthrough are also part of the Canadian Common Fund contribution. They are purchased through Orsay, along with the other ATLAS LAr cables, from Axon. A Memorandum of Understanding for the procurement of the endcap pigtail cables has been signed by Orsay and ATLAS-Canada. A detailed procurement schedule has been developed, and reception of pigtails in Victoria is now (at year-end) 74% complete. Reception is expected to be completed early in 2002.

Pin carriers

Extensive and detailed tests comparing the ceramic and glass pin carrier technologies were made in 1997 and 1998. Both technologies were found to be suitable for our project. A glass technology pin carrier was welded to a test flange in Canada and subjected to a burst test in CERN. It was found not to be affected by a pressure of up to 250 bar. The green light was given at the PRR to purchase glass technology pin carriers made of low inclusion 304L stainless steel. The order was placed in June, 1999. Procurement problems with

the low inclusion stainless steel caused approximately six months' delay. Further delays occurred when the procured steel proved to be unsuitable for hermetic seal use. After extensive studies and tests, coordinated by Tom Muller (BNL) and the manufacturer, a source of suitable stainless steel was found. Pin carrier production resumed in February, 2001. We have now (at year-end) received 77% of the required pin carriers. Reception is expected to be completed early in 2002.

Other components

Other components (bellows, flanges, funnels, VCR T-glands and heater plate parts) are all in stock.

Assembly and installation

A total of 50 feedthrough assemblies plus 5 spares must be produced (see Fig. 15). From the experience gained with the prototype construction and tests and with the production of the first assemblies, a detailed assembly procedure, quality plan and quality assurance plan have been developed and refined. These include the description of the testing of components from their arrival in Victoria through the completion of feedthrough units. Complete material traceability is ensured through the use of detailed traveller sheets.

The funnel and cold flange of each feedthrough assembly are part of the cryostat pressure vessel. An officially licensed company is doing the welding and extensive testing to conform to accepted welding code. Special test sections of a feedthrough assembly have been made for TIS (CERN Safety Group) tests. Final TIS approval of our welding plan has been obtained.

The shipment of feedthrough assemblies to CERN is done by air freight. Shipping crate construction follows the feedthrough assembly production. Upon arrival at CERN, each feedthrough assembly is subjected to an ambient temperature leak test and a basic electrical test. We are responsible for these tests. The required testing equipment was commissioned at CERN in October, 2001, when the first feedthrough assemblies arrived at CERN.

Fig. 15. Vacuum cables being installed on a feedthrough by Paul Birney (TRIUMF) at the University of Victoria.

The installation of the feedthrough assemblies on the cryostat is a delicate and complex operation. Although the feedthrough installation is not a Canadian responsibility, our group is expected to actively assist during the operation. In particular, given the softness of the pins, members of our team will manually connect the so-called warm cables that join the outside of the ambient flange to the electronics crate baseplane. Each feedthrough assembly, once welded on the cryostat, must also be electrically tested. Furthermore, we must assist during the leak testing of the cryostat.

Project schedule

The current ATLAS schedule indicates that the endcap cryostats will be ready for feedthrough integration approximately in March, 2002 and October, 2002. The endcap signal feedthrough project is on track with the ATLAS schedule. As of the end of 2001, 23 feedthrough assemblies have been produced and tested, and 21 are at CERN. An average production rate of 3 assemblies per month, including tests, is expected (a peak production rate of 3 assemblies in 22 days was achieved). It is expected that Canada's involvement in the feedthrough installation will end during 2003 with the connection of the warm cables to the ambient flange.

Canadian participants in ATLAS

Investigators: J. McDonald, J. Pinfold, M. Vincter (Alberta); D. Gingrich, P.W. Green (Alberta/TRIUMF); J. Armitage, M. Dixit, G. Oakham (Carleton); P. Depommier, C. Leroy, J.-P. Martin (Montréal); G. Azuelos (Montréal/TRIUMF); G. Couture (Montréal/UQAM); M.C. Vetterli (SFU/TRIUMF); D.C. Bailey, R.S. Orr, P. Sinervo, W. Trischuk (Toronto); P. Krieger, J.F. Martin (Toronto/IPP); M. Losty, C. Oram (TRIUMF); D. Axen (UBC); A. Astbury, R. Keeler, M. Lefebvre (Victoria); R. McPherson, R. Sobie (Victoria/IPP); S. Bhadra (York).

Collaborators: S. Liu, R. Soluk, S. Wheeler (Alberta); B. Caron (Alberta/TRIUMF); M. Khahkzad (Carleton); R. Mehdiyev (Montréal); Kyung Kwang Joo (Toronto); S. Chekulaev, H. Stenzel, M. Wielers (TRIUMF); M. Fincke-Keeler, N. Kanaya (Victoria).

Graduate students: N. Buchanan, L. Chen, C. Cojoocaru, B. Dowler, J. de Jong, R. McDonald, Wei-Yuan Ting (Alberta); G. Belanger, B. Williams (Carleton); P.H. Beauchemin, G. Fubiani, M.H. Genest, C. Lebel, R. Mazini, F. Marullo, P. Roy (Montréal); K. Martens (Toronto); M. Dobbs, T. Ince, V. Singh (Victoria).

The BaBar experiment at the Stanford Linear Accelerator Center

(C. Hearty, UBC)

Introduction

BaBar is an experiment to study the electroweak sector of particle physics using B mesons produced at the high-luminosity e^+e^- collider PEP-II. The primary physics goal is to observe and quantify CP violation in B mesons, but more generally, it is to test the standard model description of electroweak physics and to look for new physics beyond the standard model. The charged weak force is described by the CKM matrix in the standard model, and the central physics goals of BaBar are often described in terms of overconstraining the "unitarity triangle", a geometrical representation of the CKM matrix. In particular, a non-zero angle in the unitarity triangle would imply CP violation.

The BaBar detector was designed, constructed and assembled prior to the start of the first data run in October, 1999. The current data run started in January, 2001 and will continue until summer, 2002. The drift chamber, one of six major detector systems, was constructed at TRIUMF. It is performing well: the observed mass resolution for J/ψ mesons decaying to muon pairs is 12.3 ± 0.3 MeV/c^2, consistent with the value of 12.0 ± 0.1 MeV/c^2 predicted by simulation (Fig. 16).

Observation of CP violation in B mesons

2001 was a productive year for BaBar, with numerous interesting physics results. The most exciting of these is the first observation of CP violation in B mesons. This measurement compares the decay rates of B^0 and $\bar{B}^0$ mesons to CP eigenstates, where the rates would be identical if CP were a good symmetry of nature. B mesons at BaBar are produced in B^+B^- or $B^0\bar{B}^0$ pairs in the decay of an $\Upsilon(4S)$ resonance. The events useful in the asymmetry analysis are those in which one B^0 meson decays to a CP eigenstate, such as $J/\psi K_S$, and the other decays in such a way that it can be "tagged". Tagging consists of partially reconstructing the decay products for the purpose of detecting whether the original meson was a B^0 or a $\bar{B}^0$.

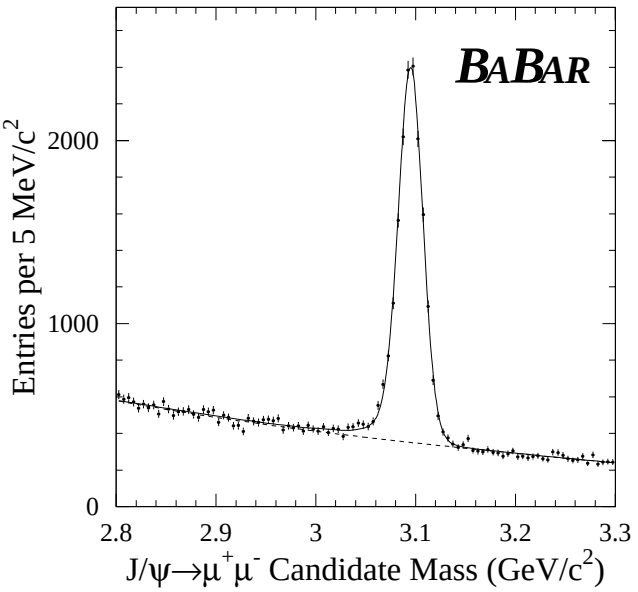

Fig. 16. J/ψ mesons reconstructed in BaBar via decay to a muon pair.

The most recent results use a sample of 62 million $\Upsilon(4S)$ decays recorded in 56 fb^{-1} of data. A total of 1848 B^0 meson candidates are reconstructed in the following final states: $J/\psi K_S$, $J/\psi K_L$, $\psi(2S)K_S$, $\chi_{c1}K_S$ and $J/\psi K^{*0}$, with an average purity of 80%. This total includes only those events in which the other B^0 has been tagged. The effective tagging efficiency (including the dilution of the signal due to incorrect tagging) is 25%.

The asymmetry between B^0 and $\bar{B}^0$ is illustrated in Fig. 17. The corresponding measurement of the unitarity triangle is $\sin 2\beta = 0.75 \pm 0.09$ (statistical) $\pm$ 0.04 (systematic). This clearly demonstrates the violation of CP in the B system.

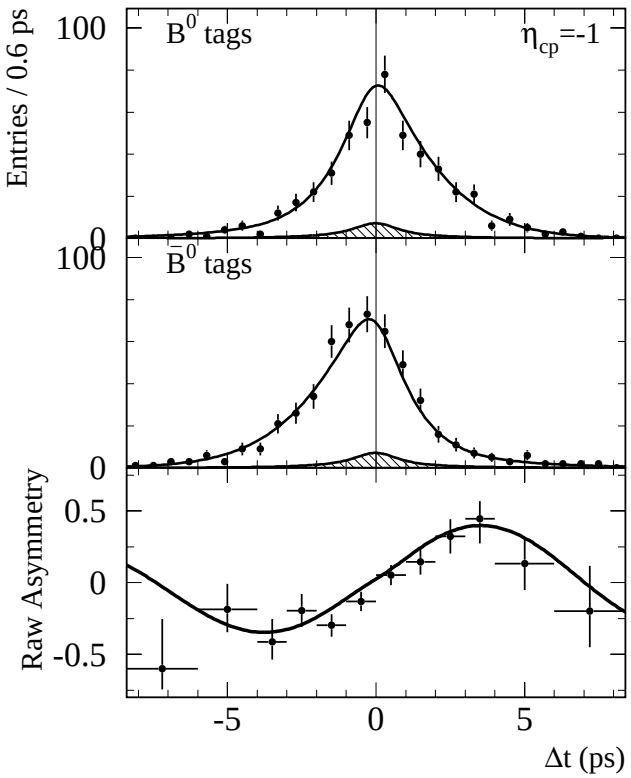

Fig. 17. Number of CP final state candidates (top) with a B^0 tag N_{B^0}, (middle) with a $\bar{B}^0$ tag $N_{\bar{B}^0}$, and (bottom) the raw asymmetry $(N_{B^0} - N_{\bar{B}^0})/(N_{B^0} + N_{\bar{B}^0})$, as functions of the time difference between the signal and tag decay.

Activities of the local group

The local group has led the analysis for two publications in 2001. One analysis was the first observation of the direct production of J/ψ mesons in e^+e^- annihilation. These mesons were distinguished from the much more copious production in B decay by using data recorded at energies below the threshold for $B\bar{B}$ production, and by using J/ψ mesons with momentum higher than kinematically possible for B decay. This analysis has helped illuminate the production mechanisms of heavy quarkonia, such as non-relativistic QCD.

The second paper determined the branching fractions of the $\psi(2S)$ to e^+e^- and $\mu^+\mu^-$. The $\psi(S)$ mesons are widely used in reconstructing B mesons, and the previous precisions of these quantities were a limiting factor in a number of analyses.

The group has more recently started collaborating with colleagues at the University of Victoria on a search for the as-yet undiscovered decay $B \to K\nu\bar{\nu}$. This is a rare, flavour-changing neutral current process that occurs via loops in the standard model. It is a theoretically clean process with a rate that is sensitive to supersymmetry or other physics beyond the standard model.

Outlook

The success of BaBar is due largely to the success of PEP-II, which has consistently delivered luminosity above the design value. In 2001, for example, BaBar recorded 39.5 fb^{-1} of data, compared to a design value of 30 fb^{-1}. This trend is anticipated to continue. The high luminosity will permit BaBar to determine a second angle of the unitarity triangle and to accurately measure the length of its sides. It will also permit a wide range of searches for rare B decays, possibly exposing new physics.

BNL E787/949/KOPIO
Measurement of $K \to \pi\nu\bar{\nu}$ and other rare decays

(D. Bryman, UBC)

The rare kaon decays $K^+ \to \pi^+\nu\bar{\nu}$ and $K_L^0 \to \pi^0\nu\bar{\nu}$ offer unique opportunities to scrutinize higher order phenomena associated with quark mixing and charge-parity (CP) non-invariance. Initial data from Experiment E787 at Brookhaven National Laboratory (BNL) yielded the first evidence for the $K^+ \to \pi^+\nu\bar{\nu}$ decay. This year the final result from E787 was reported [Adler *et al.*, Phys. Rev. Lett. **88**, in press] based on the full data set which doubled the previously reported sensitivity. The branching ratio remains consistent with the standard model (SM) expectation.

To fully explore the possibility of new physics, or to make a precise measurement of the $t-d$ quark coupling $|V_{td}|$, requires a new measurement capable of a single event sensitivity of $\mathrm{B}(K^+ \to \pi^+\nu\bar{\nu}) = (8-14)\times 10^{-12}$, roughly an order of magnitude below the SM prediction. Substantial upgrades to the E787 detector system have been made during the past two years in preparation for a continued experiment, E949, aimed at reaching this sensitivity. In 2001, E949 commenced with a brief engineering run starting in September. The Alternating Gradient Synchrotron (AGS) will be operated for E949 in conjunction with its role as injector to the Relativistic Heavy Ion Collider (RHIC). Injection is planned roughly twice per day, leaving more than 20 hours per day available for AGS slow extracted beam. With the completion of E949, the possibility of an inconsistency with the SM prediction of $\mathrm{B}(K^+ \to \pi^+\nu\bar{\nu})$ will be fully explored, or the important top-down quark mixing parameter will be determined to a precision of 15–30% if the SM expectation is confirmed.

Despite an enormous worldwide effort in B physics, it has become evident that the K sector can yield the single most incisive measurement in the study of direct CP violation through a measurement of the branching ratio for $K_L^0 \to \pi^0\nu\bar{\nu}$. In the context of the SM $\mathrm{B}(K_L^0 \to \pi^0\nu\bar{\nu})$ is a unique quantity which directly measures the common area of the CKM unitarity triangles, i.e. the physical parameter that characterizes all CP violation phenomena, or, alternately, the height of the triangle. Measurements of both $\mathrm{B}(K_L^0 \to \pi^0\nu\bar{\nu})$ and $\mathrm{B}(K^+ \to \pi^+\nu\bar{\nu})$ will allow the unitarity triangle to be precisely reconstructed from K decay information alone. Thus, a complete picture of standard model CP violation in the K system will result and a comparison with comparably precise measurements anticipated from the B sector will be enabled.

The challenges of measuring $\mathrm{B}(K_L^0 \to \pi^0\nu\bar{\nu})$, expected to occur at 3×10^{-11}, have been taken up by the KOPIO collaboration. KOPIO will employ a low energy, time structured K_L^0 beam from the BNL AGS to allow determination of the incident kaon momentum. The goal of KOPIO is to obtain about 50 events with a signal to background ratio of at least 2:1. This will yield a statistical uncertainty in the measurement of the area of the CKM unitarity triangle of less than 10%. KOPIO is presently in an R&D phase.

Final results from E787

The decay $K^+ \to \pi^+\nu\bar{\nu}$ is very sensitive to the magnitude of the coupling of top to down quarks, V_{td}, in the Cabibbo-Kobayashi-Maskawa quark mixing matrix. In the context of the standard model (SM), the predicted branching ratio is $\mathrm{B}(K^+ \to \pi^+\nu\bar{\nu}) = 0.75 \pm 0.29 \times 10^{-10}$ [Buras, preprint hep-ph/0101336 (2001); Buras and Fleischer, preprint hep-ph/0104238 (2001); Buchalla and Buras, Nucl. Phys. **B548**, 309

(1999)]. In the earlier E787 study, a single event consistent with the decay $K^+ \to \pi^+\nu\bar{\nu}$ at a branching ratio of $B(K^+ \to \pi^+\nu\bar{\nu}) = 1.5^{+3.5}_{-1.2} \times 10^{-10}$ was found [Adler *et al.*, Phys. Rev. Lett. **84**, 3768 (2000) and Phys. Rev. Lett. **79**, 2204 (1997)].

The observable signature for $K^+ \to \pi^+\nu\bar{\nu}$ decay from kaons at rest involves only the π^+ track and π^+ decay products. Major background sources include the two-body decays $K^+ \to \mu^+\nu_\mu$ ($K_{\mu 2}$) and $K^+ \to \pi^+\pi^0$ ($K_{\pi 2}$), pions scattered from the beam, and K^+ charge exchange (CEX) reactions resulting in decays $K^0_L \to \pi^+ l^- \bar{\nu}_l$, where $l = e$ or μ. In order to make an unambiguous measurement of $B(K^+ \to \pi^+\nu\bar{\nu})$, it is advantageous to suppress all backgrounds well below the signal level.

The additional data discussed here were acquired during the 1998 run of the AGS. The kaons were stopped in a scintillating fibre target used for kaon and pion tracking. Measurements of the momentum (P), range (R), and kinetic energy (E) of charged decay products were made using the target, a central drift chamber, and a cylindrical range stack (RS) with two layers of tracking chambers embedded in it, all within a 1 T solenoidal magnetic field. The $\pi^+ \to \mu^+ \to e^+$ decay sequence from pions which came to rest in the RS was observed using 500 MHz transient digitizers. Photons were detected in a nearly 4π 14-radiation-length-thick calorimeter array of either lead/scintillator sandwich or undoped CsI crystals.

To be accepted as a $K^+ \to \pi^+\nu\bar{\nu}$ candidate, a decay particle must be positively identified as a π^+ by comparing P, R, and E measurements, and by observation of the $\pi^+ \to \mu^+ \to e^+$ decay sequence. Events containing other decay products including photons or beam particles were eliminated by detectors covering 4π sr. The search was restricted to the measured momentum region $211 < P < 229$ MeV/c between the $K_{\mu 2}$ and $K_{\pi 2}$ peaks. The maximum pion momentum from $K^+ \to \pi^+\nu\bar{\nu}$ decays at rest is 227 MeV/c.

Some new aspects of the analysis of the 1998 data set include applications of neural network techniques in the particle identification process and incorporation of improved routines to detect large angle scattering of particles in the range stack. In the 1998 exposure, the effective number of kaon stops was $N_{K^+} = 2.7 \times 10^{12}$, approximately 82% as large as all previous E787 data sets, and the acceptance was determined to be $0.173 \pm 0.005 \pm 0.009\%$ giving a single event sensitivity of 2.14×10^{-10}.

The data analysis obtained detailed estimates of all backgrounds prior to examining the pre-determined signal region. In order to evaluate observed events, the parameter space of observables was subdivided into 7500 bins with differing levels of expected backgrounds. To confirm the background estimates, the selection criteria were relaxed to allow about 14 times higher background, and all bins except those in the final signal region were examined. Two events were observed, in agreement with the number of expected background events $\Sigma_{i=487}^{7500} b_i = 0.9 \pm 0.7$ for this region.

The signal region was defined to include the first 486 bins and was not examined until the final step in the analysis procedure. For the 1998 data set, the final candidate selection requirements were similar to those used previously, although more stringent track reconstruction criteria were imposed. Following the background study, the signal region was examined yielding one candidate event (event C). The kinematic values are $P = 213.8 \pm 2.7$ MeV/c, $R = 33.9 \pm 1.2$ cm (in equivalent cm of scintillator), and $E = 117.1 \pm 3.6$ MeV. A display of this event is shown in Fig. 18. Close inspection of Event C indicates that it is consistent with being due to $K^+ \to \pi^+\nu\bar{\nu}$ decay.

The combined result for E787 data taken between 1995 and 1998 is shown in Fig. 19, the range vs. kinetic energy of events surviving all other cuts. In Fig. 19 the box represents the signal region in which two events, A(1995) and C(1998) appear. Using a likelihood ratio technique [Junk, Nucl. Instrum. Methods **A434**, 435 (1999)] to determine the best estimate of the branch-

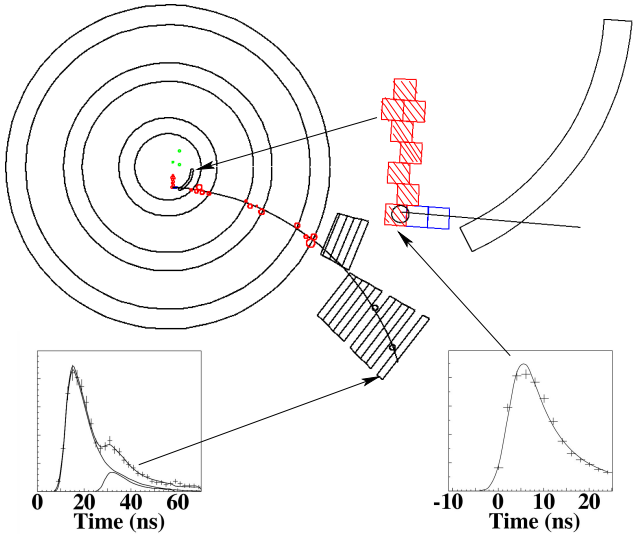

Fig. 18. Display of candidate event C. On the top left is the end view of the detector showing the track in the target, the drift chamber, and the range stack. On the top right is a blow-up of the track in the target, where the hatched squares represent target fibres hit by the K^+ and the open squares indicate those hit by the π^+; a trigger scintillator that was hit is also shown. The lower right-hand box shows the digitized signal in the target fibre where the kaon stopped, indicating no additional activity. The pulse was sampled every 2 ns (crosses) and the solid line is a fit. The lower left-hand box shows the digitized $\pi \to \mu$ decay signal in the scintillator where the pion stopped. The curves are fits for the first, second and combined pulses.

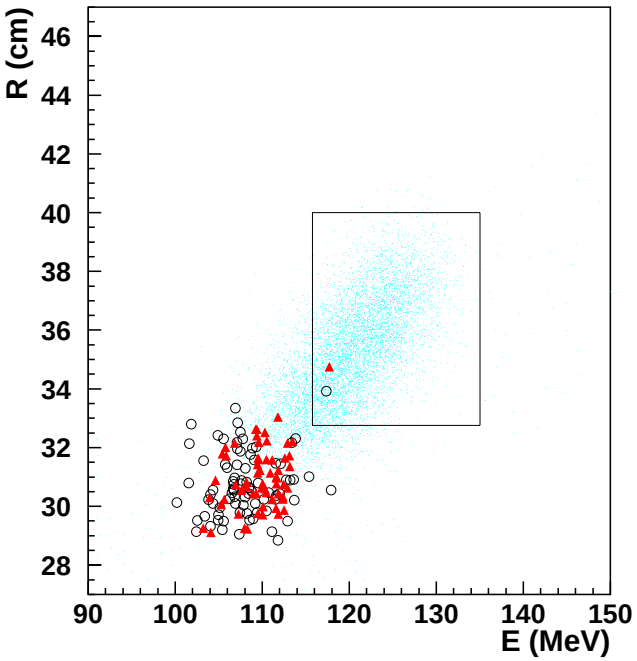

Fig. 19. Range vs. energy plot of the final sample. The circles are for the 1998 data and the triangles are for the 1995-97 data set. The group of events around $E = 108$ MeV is due to the $K_{\pi 2}$ background. The simulated distribution of expected events from $K^+ \to \pi^+ \nu\bar{\nu}$ is indicated by dots.

ing ratio based on two observed events with their associated signal-to-background estimates, the determined acceptance, the number of K^+ incident on the target, and the expected background levels, the result is $\mathrm{B}(K^+ \to \pi^+ \nu\bar{\nu}) = 1.57^{+1.75}_{-0.82} \times 10^{-10}$ (68% C.L.). This result would be consistent with being due entirely to background only at the level of 0.02%.

Bounds obtained on $|V_{td}|$ from $\mathrm{B}(K^+ \to \pi^+ \nu\bar{\nu})$ are $0.007 < |V_{td}| < 0.030$ (68% C.L.) or $0.0051 < |V_{td}| < 0.033$ (90% C.L.) and do not require knowledge of V_{ub} or ϵ_K. Alternatively, one can extract corresponding limits on the quantity $|\lambda_t|$ ($\lambda_t \equiv V_{ts}^* V_{td}$): $2.9 \times 10^{-4} < |\lambda_t| < 1.2 \times 10^{-3}$. In addition, the bounds $-0.88 \times 10^{-3} < Re(\lambda_t) < 1.2 \times 10^{-3}$ can be obtained. For $Im(\lambda_t)$, an upper limit of $Im(\lambda_t) < 1.1 \times 10^{-3}$ (90% C.L.) is found. The bounds on λ_t are derived without reference to the B system or to measurements of ϵ_K or ϵ'/ϵ, and are of particular interest because $Im(\lambda_t)$ is proportional to the area of the unitarity triangle.

The limit found in the search for decays of the form $K^+ \to \pi^+ X^0$, where X^0 is a neutral weakly interacting massless particle [Wilczek, Phys. Rev. Lett. **49**, 1549 (1982)], is $\mathrm{B}(K^+ \to \pi^+ X^0) < 0.59 \times 10^{-10}$ (90% C.L.), based on zero events observed in a $\pm 2\sigma$ region around the pion kinematic endpoint.

Progress has also been made to access the region below the $K_{\pi 2}$ peak. A complete analysis of data taken in 1996 has been performed at BNL leading to a background of 1.0 ± 0.5 events expected at a sensitivity level of approximately 10^{-9}, roughly an order of magnitude below the previous E787 results. Final results are in preparation for publication [Adler *et al.*, e-print archive: hep-ex/0201037].

E787 has also studied numerous other rare K and π decays and performed searches for many as-yet unobserved processes. In 2001 and late 2000, results were reported for the first high statistics measurement of the direct emission component of the radiative decay $K^+ \to \pi^+ \pi^0 \gamma$ [Adler *et al.*, Phys. Rev. Lett. **85**, 4856 (2000)], as well as searches for the decays $K^+ \to \pi^+ \gamma$ [Adler *et al.*, Phys. Rev. **D** (in press)] and $K^+ \to \pi^+ \pi^0 \nu\bar{\nu}$ [Adler *et al.*, Phys. Rev. **D63**, 032004 (2001)].

E949

E949 is based on incremental upgrades to the techniques and technology of E787. Since E949 is expected to be the primary (or only) AGS user, the proton beam on target is intended to have an intensity of 65×10^{12} in a 4 s spill, giving a duty factor of 64%. This translates into an effective luminosity improvement of 56% over previous running conditions while keeping instantaneous rates at the same level. E949 running with higher instantaneous rates will also be attempted to increase the sensitivity.

Enhancements to the detector included improvements to the range stack inner layers and trigger counters (manufactured in Russia), elements of the photon veto systems, upgrade of the trigger system, and improvements to the data acquisition system for higher rates.

For E949, the TRIUMF group constructed a new set of more highly segmented beam counters in order to achieve improved spatial resolution where the incoming particle enters the target, and improved photon vetoing efficiency for photons coming back along the beam line. In E787 the escape of these photons was a major contributor to the overall photon detection inefficiency. The total number of hodoscope elements was doubled and re-designed to improve the $X - Y$ spatial resolution. Each hodoscope element is read out by 3 wavelength shifting (WLS) double-clad 1 mm diameter fibres. In addition, a new "ring veto" will allow the detection and vetoing of particles which enter counter B4 near its outside edge.

In order to improve photon detection efficiency, the 3-radiation-length (X_0) thick lead glass detector used in E787 has been replaced by a copper/scintillator sandwich active degrader (AD) of larger diameter. This detector consists of 40 layers of 2.2 mm thick copper interposed with 2 mm thick scintillator to give a total thickness of 6.3 X_0. The scintillators are split into 12 azimuthal segments. Each segment is read out via

WLS fibres. The 12-fold segmentation was chosen to minimize the likelihood that a photon signal would be hidden by the much larger pulse deposited by an incoming kaon. Further photon detection is provided by a new upstream photon veto (UPV) counter located in front of the entrance to the magnet. This detector is a 3 X_0 lead/scintillator sandwich, also read out by WLS fibres with an aperture to allow the incident kaon beam to pass through without interacting.

The TRIUMF-built central drift chamber (UTC) was repaired to improve cathode foil signals which were affected by deteriorating foil-connector joints due to micro-cracks in the conductive epoxy. A longstanding problem associated with the cathode charge measurement system, caused by ADCs malfunctioning due to a tiny wrong-polarity undershoot from large pulses, was addressed by replacing the 768 pre-amplifiers and post-amplifier/discriminator electronics. As an additional benefit, the noise level in the ADC measurements dropped by a factor of 2–3, and improvements in the z-position resolution were obtained. In addition, we modified the anode front end electronics (1152 channels) to improve the signal transmission.

Several of the limited-streamer mode straw tube detectors (RSSC) required repair and a new electronics front end system was implemented to improve the performance of the z-coordinate measurement used to suppress backgrounds from scattered muons. The poor resolution was due to low pulse height time-walk effects and a new preamplifier-dual-discriminator front end system was designed and constructed. Tests indicate improvements in resolution by a factor of three to about 1.5 cm. This improved performance of the RSSCs will translate into much improved muon background rejection in E949.

The TRIUMF group participated substantially in many other E949 upgrade projects. Since the TRIUMF group maintains the E787/E949 software systems, major upgrades of the primary analysis shell were implemented to accommodate new hardware systems.

For the E949 engineering run in September–October, 2001, most of the upgrade elements were in place and commissioned. An 8–12 week data run is scheduled to begin in February, 2002.

KOPIO

The KOPIO experiment is designed to observe and measure the rate of the decay $K_L^0 \to \pi^0\nu\bar{\nu}$ by observing a large sample of clean events. This goal will allow the SM CP violation parameter, η, to be determined to 15% accuracy with minimal contributions from background or systematic effects.

In the KOPIO design, a 500 μsr solid angle neutral beam is extracted at 45° to produce a "soft" K_L spectrum peaked at 0.65 GeV/c; kaons in the range from about 0.5 GeV/c to 1.3 GeV/c will be used. Downstream of the final beam collimator is a 3.5 m long decay region which is surrounded by the main detector. Approximately 16% of the kaons decay, yielding a decay rate of about 25 MHz. The beam region is evacuated to a level of 10^{-7} torr to suppress neutron induced π^0 production. The decay region is surrounded by an efficient Pb/scintillator photon detector which serves to veto photons and charged particles. In the forward detection region the primary photon detector system, illustrated in Fig. 20, consists of two sections: a fine grained preradiator (PR) in which the photons are converted, followed by an 18 X_0 calorimeter in which the remaining energy of the photon shower is measured. The PR functions to measure the photon positions and directions accurately in order to allow reconstruction of the K_L decay vertex, while also contributing to sufficient energy resolution. The calorimeter is constructed using Pb/scintillator layers. In the barrel and upstream regions, a Pb/scintillator combination will also be used to obtain high veto efficiency. Downstream of the main π^0 detector, a beam hole photon counter ("beam catcher") consists of Čerenkov detectors designed to be insensitive to neutrons.

The Canadian group's main hardware contribution to KOPIO is the PR detector system which consists of 64 0.03 X_0 layers (total effective thickness of 2 X_0), each with plastic scintillator, metal converter and dual-coordinate drift chambers. The requirements include a photon angular resolution of approximately 25 mr, a photon conversion efficiency of about 0.7 (2.0 X_0), a good measurement of the deposited energy, and as short as possible linear extent so as to limit shower size at the calorimeter.

The principle employed is to measure the positions and angles of the first e^+e^- pair following photon conversion in a series of thin converter/detector modules. Each PR module consists of an inactive converter material, a dual coordinate drift chamber (anode wires and cathode strips) and a scintillator. The chambers provide the position measurements and the scintillation counters are used for triggering, timing, and energy loss measurement. To keep multiple Coulomb scattering at the 25 mr level the PR layers are thin ($\leq$0.034 X_0), are separated by about 1 cm, and have position resolution of between 150 and 200 μm. In addition, the energy deposited in the preradiator will be measured with sufficient precision to allow the full energy measurement (including the PR and the calorimeter) to be better than $3.0\%/\sqrt{\mathrm{E}}$ (GeV).

This method of measuring the photon directions has been confirmed experimentally by KOPIO in a proof-of-principle measurement in a tagged photon beam at BNL LEGS, and the expected angular

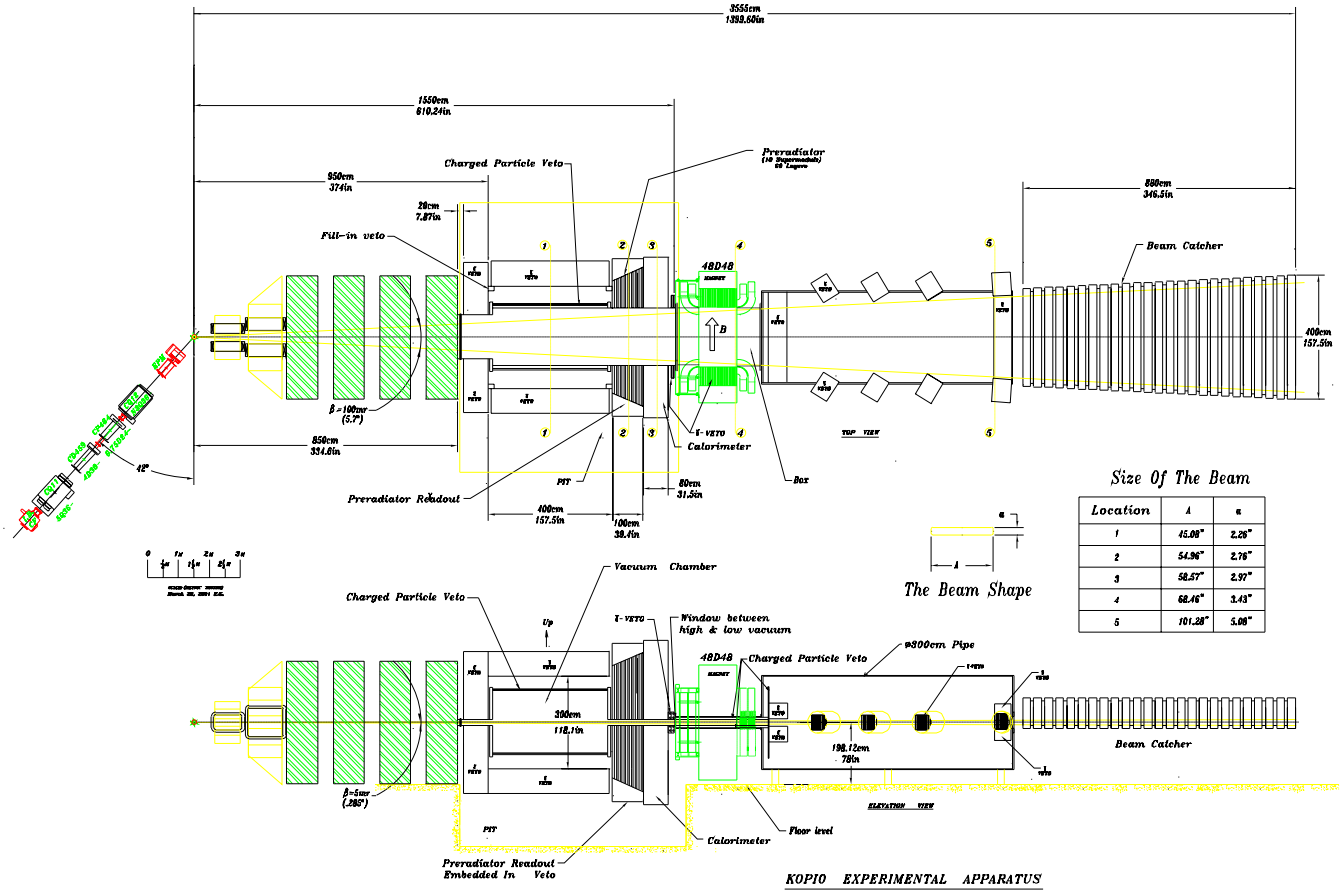

Fig. 20. $K_L^0 \to \pi^0 \nu\bar{\nu}$ detector.

resolution for photons was determined by GEANT simulation with 3.4% X_0 per layer and assuming 150 μm position resolution for the measurements of e^+e^- pairs.

Several chamber prototypes are being constructed. Five small (8 cm × 15 cm) chambers were fabricated to test the basic cell design and construction technique mentioned above. These gave the expected level of performance. The maximum drift time using an Ar/ethane mixture was measured to be 70 ns with full efficiency. For CF_4/isobutane mixtures, we expect 35 ns maximum drift. These chambers were assembled in a stack to study tracking properties using different chamber parameters. Two larger (30 cm × 30 cm) chambers were also constructed and are being readied for testing.

Other chamber structures will be full length devices in each of the anode and cathode dimensions (200 cm × 20 cm) primarily for electronics development. The next step will be chambers approximately 50 cm × 50 cm in size to be used in stacks of eight to test the tracking and energy measurement performance in test beams at TRIUMF and BNL LEGS using preproduction electronics. The final prototype will be a full size pre-production model.

The anodes and cathodes from each preradiator layer will be read out and digitized individually at the chamber; only digitized information will be taken from the chamber area. The electronics is designed to be a fully pipelined dead-timeless system. The analogue electronics for the cathode strips contains a charge amplifier, shaper, and a 10-bit 40 MHz A/D converter followed by a programmable logic device which includes memory, peak detection (to represent the charge integral), pedestal subtraction, data sparsification and readout. The timing electronics employs a fast amplifier and a discriminator followed by a time-memory-cell VLSI chip. We are investigating the use of several ASICs designed for ATLAS and CMS.

The scintillator planes interposed between the chambers will be read out in strips using wavelength shifting fibres. The fibres will be oriented to read alternating coordinates in vertical, horizontal and diagonal directions. The latter will be used to help resolve multiple hits on the other two planes. The scintillator planes also extend beyond the preradiator wirechamber dimensions to provide a veto halo for photons whose showers are not fully contained in the preradiator/calorimeter.

The scintillator planes need to be of highly uniform thickness and flatness in order to also serve as a vital structural element supporting the wire chambers. The possibility of using extrusion techniques to manufacture "planks" which can be bonded together into the large planes is being investigated.

The HERMES experiment

(C.A. Miller, S. Yen, TRIUMF; M.C. Vetterli, SFU/TRIUMF; M.G. Vincter, Alberta)

The HERMES experiment has been recording data for 6 years, investigating primarily the spin structure of the nucleon, but also a rich variety of other topics in QCD physics. The unique capabilities of the experiment include a pure nuclear-polarized atomic gas target in a 27.5 GeV stored polarized electron beam. The spectrometer has acceptance sufficient to detect hadrons associated with the scattered electron, with complete hadron identification by a dual-radiator ring-imaging Čerenkov detector. An extensive data set has been accumulated, which is under continuing analysis. The final results are expected to achieve the main goals set out in the original proposal. Simulations based on the preliminary results indicate that the flavour separation of the polarized quark distributions will be complete, with sensitivity to even a $\bar{u}/\bar{d}$ sea flavour asymmetry at a precision that can distinguish between model predictions. These preliminary results are expected to be released in early 2002. In the meantime, several new HERMES results have appeared in both polarized and unpolarized QCD physics, many benefitting from the much thicker unpolarized gas targets that are now used near the end of every HERA beam fill.

Beam spin transfer to Λ's

It has been proposed that one could obtain additional information on the polarized quark distributions in the baryons of the spin 1/2 octet through the production of Λ hyperons in polarized deep-inelastic lepton scattering. By measuring the polarization of the Λ's that are likely to have originated from the struck quark (so-called "current fragmentation"), the longitudinal spin transfer $D^{\Lambda}_{LL'}$ can be determined. This quantity is defined as the fraction of the virtual photon polarization transferred to the Λ. In the naive quark parton model (QPM) the spin of the Λ is entirely due to the strange quark, and the up and down quark polarizations are zero. On the other hand, assuming SU(3) flavour symmetry, the up, down and strange quark distributions (and fragmentation functions) for the Λ can be related to those in the proton. If existing data on hyperon decays and polarized structure functions of the nucleon are interpreted in the framework of SU(3) symmetry, the first moments of the polarized up and down quark distributions in the Λ can be estimated to be about -0.2 each. If one assumes in addition that quark helicity is conserved in the fragmentation process, one obtains this same negative value for the expected spin transfer from a struck up or down quark to the Λ. A measurement of the spin transfer thus has the potential to provide information on the spin structure of the Λ hyperon.

Longitudinal spin transfer in Λ production has previously been studied at the Z^0 pole at LEP. In the standard model, strange quarks (or quarks of charge $-1/3$ in general) produced via Z^0 decays have an average polarization of -0.91. Both the ALEPH and OPAL collaborations have reported a measurement of the Λ polarization of about -0.3 for $z > 0.3$. (Here, z is the fraction of the available energy carried by the Λ.) These data are consistent with the naive constituent quark model, but their interpretation is not unique as all three light quark flavours contributed significantly to the production of Λ hyperons, with the strange quark playing the dominant role. By contrast, Λ production in deep-inelastic lepton scattering is dominated by scattering on up quarks. Hence such experiments with a polarized lepton beam provide a means to distinguish between the various models of the Λ spin structure, and to investigate further the degree of helicity conservation in the fragmentation process.

The polarization of Λ hyperons can be measured via the weak decay channel $\Lambda \to p\pi^-$, through the angular correlation of the final state. HERMES has extracted about 10^4 Λ events from the 1999/2000 data sets. In the current fragmentation region, where the Feynman x_F variable is positive, the spin transfer is found to be consistent with zero: $D^{\Lambda}_{LL'} = 0.04 \pm 0.08(\text{stat}) \pm 0.03(\text{syst})$, again supporting the naive quark model. On the other hand, other experiments in the target fragmentation region ($x_F < 0$) result in negative values, as shown compared to the HERMES data in Fig. 21. The neutrino results suggest a mechanism in which the spin of $s\bar{s}$ pairs pre-existing in the target anticorrelates with the spin of the struck quark.

Quark-hadron duality

When protons are probed by electrons at energies large compared to the proton mass with correspondingly large 4-momentum transfers ($-Q^2$), the scattering probability (summarized in the structure function $F_2(W^2, Q^2)$ where W is the invariant mass of the initial photon nucleon system) is rather simple. It exhibits the well known property of scale invariance where $F_2 \sim F_2(W^2/Q^2)$, with small corrections that are well understood from perturbative QCD. The magnitude of $F_2(W^2/Q^2)$ is proportional to the sum of the squares of the parton (quark and antiquark) charges.

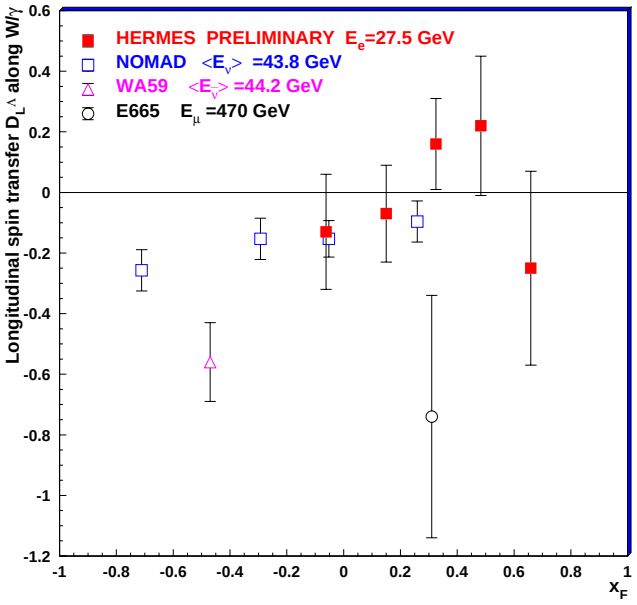

Fig. 21. Longitudinal spin transfer $D^{\Lambda}_{LL'}$ from the lepton beam to the detected Λ, from HERMES (filled symbols) and other experiments (empty symbols).

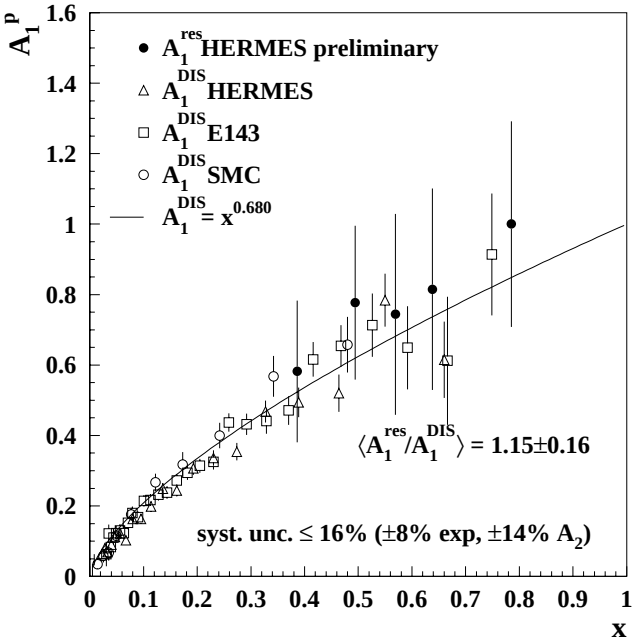

Fig. 22. Photo-absorption spin asymmetries A_1 as a function of x measured in the resonance region (filled circles). The error bars represent the statistical uncertainties; the systematic uncertainty is about 16%. The empty symbols are previous results obtained in the DIS region, and the curve represents a phenomenological fit to DIS data at $x > 0.03$.

Before the advent of QCD, Bloom and Gilman discovered an empirical property of the data, namely that the electroproduction of N^*'s at lower energies and momentum transfers averages smoothly around the scaling curve measured at large momentum transfers. During the subsequent three decades, and especially following the advent of quantum chromodynamics, this enigma has received considerable theoretical attention. The literature has primarily focused on understanding how the Q^2 dependence of resonance excitation can conspire to mimic the $x' \sim \frac{Q^2}{W^2+Q^2}$ dependence of the deep-inelastic data.

Recent precise unpolarized data from Jefferson Lab have shown that this duality is observed for both proton and neutron targets, at least for spin averaged scattering. This has sparked a renewed interest in the origin of low energy duality, and in the circumstances whereby $F_2(x')$ – whose magnitude is in proportion to the sum of the squares of the (quark and antiquark) constituent charges – can in general match with the excitation of individual resonances which is driven by the coherently summed square of constituent charges. HERMES has recently released the first experimental evidence for the validity of duality for spin degrees of freedom. Longitudinally polarized positrons were inelastically scattered from longitudinally polarized protons, with values of Q^2 between 1.2 and 12 GeV/c^2 and values of W between 1 and 2 GeV. Figure 22 shows the double-spin asymmetry of the cross section in this nucleon resonance domain, compared to the existing world data for the same observable measured in deep-inelastic scattering at larger Q^2 but at the same values of the Bjørken scaling variable x. Unlike earlier such resonance asymmetries from SLAC at lower values of Q^2, these are found to be consistent with the DIS asymmetries. This implies that the description of asymmetries in terms of quark degrees of freedom applies also in the resonance region, for $Q^2 > 1.6$ GeV/c^2.

Fragmentation functions

Much of the HERMES spin physics program depends on *semi*-inclusive DIS measurements, in which the detection of a hadron produced by fragmentation of the struck quark serves to "tag" the flavour of that quark. The interpretation of these data in turn depends on our knowledge of the fragmentation functions that describe the probabilities that a quark of a particular flavour will fragment to a particular type and charge state of hadron. There exists a large set of data on fragmentation functions, as well as phenomenological QCD-motivated parametrizations and Monte Carlo models that well represent these data. However, most of these data were measured at energies higher than the beam energy used by HERMES. Therefore, it is important to confirm that the fragmentation process is well understood also at this lower beam energy.

HERMES has recently published a study of the multiplicities of both charged and neutral pions produced in DIS. Multiplicities are closely related to fragmentation functions – they differ only due to breaking

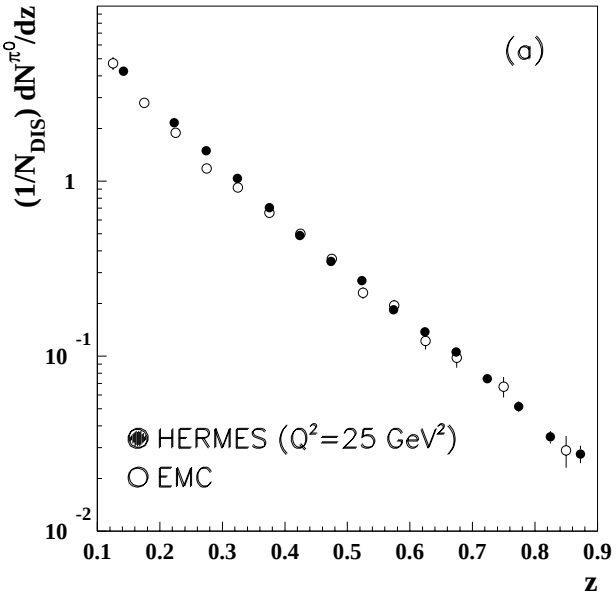

Fig. 23. Multiplicities for neutral pions from the HERMES and EMC experiments. The HERMES results have been evolved to $Q^2 = 25$ GeV^2 using the NLO QCD model of Kniehl, Kramer and Pötter [2000]. Only statistical uncertainties are shown. The systematic uncertainties are 9% for HERMES and $\leq 13\%$ for EMC.

of isospin symmetry ($D_u^\pi = D_d^\pi$, where π represents the sum of positive and negative pions) and the contributions of the strange quark. Figure 23 shows a comparison of the multiplicities of neutral pions measured by the HERMES and EMC experiments at energies that differ by about an order of magnitude. The HERMES results have been evolved to $Q^2 = 25$ GeV^2 using a NLO QCD model that unifies all of the world data on fragmentation functions. The level of agreement is remarkable. It is less so in the case of charged pions, but in this case only actual fragmentation functions are available from EMC, precluding a direct comparison.

Transverse momenta of hadrons from DIS

By studying the average transverse momenta $\langle P_\perp \rangle$ of hadrons produced by fragmentation of a quark that has absorbed an energetic virtual photon, it is possible to extract information about both the distribution in the primordial momentum component of quarks in the target nucleon transverse to its (infinite) momentum, and the transverse momentum produced in the fragmentation process. It is possible to disentangle these two contributions because that from the target tends to dominate at large values of z (the fraction of the energy of the virtual photon transferred to the hadron), indicating that the hadron probably emerged early in the fragmentation process before its direction was thereby smeared, while that from fragmentation appears at lower values of z where the hadron probably emerged after a larger number of fragmenting interactions. HERMES has recently released such

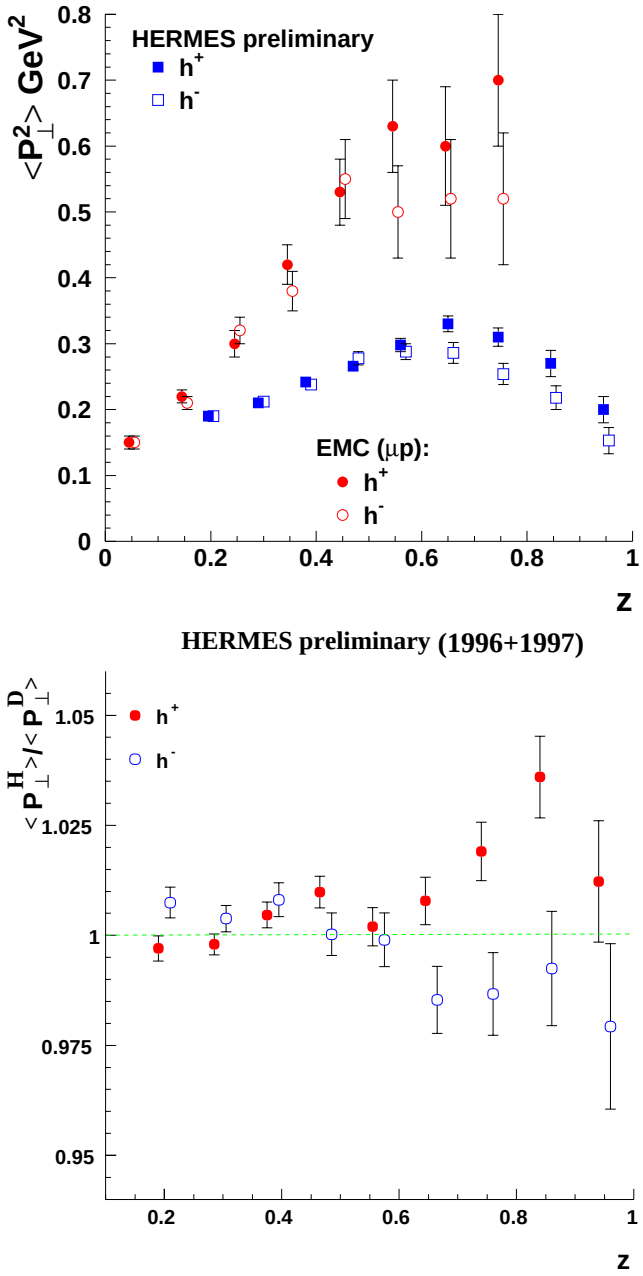

Fig. 24. The dependence of the mean square momentum component of electroproduced hadrons transverse to the direction of the virtual photon, as a function of the fraction of the photon's energy carried by the hadron. The top frame shows data from the hydrogen target, while the bottom frame shows the ratio of values for hydrogen to those for deuterium.

data with sufficient statistical precision to clearly reveal a new phenomenon. Figure 24 (top) shows these results for $\langle P_\perp^2 \rangle$ as a function of z, compared to earlier measurements from the EMC measurement at much higher energy. It is intriguing that the change of slope at large z depends on the sign of the hadron charge. Some of this effect may be due to a flavour dependence of the primordial momentum of the quarks in the

target. Up quark dominance arising from the square of the charge ratios $(+2/3)^2$ versus $(-1/3)^2$ appearing in the photoabsorption cross sections implies that positive hadrons are predominantly produced from up quarks, while negative hadrons are produced from a more equal balance of up and down. Hence the data imply that up quarks have larger primordial $P_\perp$. This is supported by the dependence on the isospin of the nucleon target, shown in Fig. 24 (bottom).

Unanticipated discoveries revealed by the existing HERMES data, together with recent dramatic theoretical progress in the understanding of QCD bound states through the exploitation of exclusive reactions, have inspired a revitalized experimental program for HERMES. This program has been approved by the DESY Programme Review Committee (PRC), leading to a promise by DESY that HERMES can run at HERA through 2006. First on this agenda is a measurement of transversity – the last unmeasured leading-twist structure function of the nucleon. In preparation for this, during the 9-month long shutdown of the HERA accelerator in 2001 for the Luminosity Upgrade, a transversely-polarized atomic gas target has been installed, and is now operational. The spectrometer is also ready, including a new silicon tracker close to the target – the "Λ Wheels". Among other advantages, this tracker will greatly enhance the acceptance for decay products of Λ hyperons, whose self-analyzing polarization carries information about the polarizations of target quarks.

The HERMES Collaboration is still building for the future. Reflecting the intense current interest in unambiguously identifying exclusive processes, the DESY PRC has now approved a proposal to construct a new recoil detector to provide large acceptance for low energy recoil target nucleons from such reactions. It is planned to be ready for running in 2004. Most of the funding is now in place. Also, the Collaboration has been strengthened by the addition of several new institutes. These include Giessen, Glasgow, IHEP Protvino, Warsaw, and soon Beijing. The Canadian group has recently welcomed two new research associates, who are focusing on extracting more physics results from the wealth of HERMES data.

KEK Expt. 246 and 470 (Japan-Russia-Canada-Korea-U.S.A. Collaboration)
Kaon decay studies
(M.D. Hasinoff, UBC; J.A. Macdonald, B. Shin, TRIUMF)

The apparatus that was constructed at the KEK 12 GeV Proton Synchrotron (PS) for the search for T-violation in the transverse polarization (P_T) of muons in $K^+ \to \pi^0\mu^+\nu_\mu \quad (K^+_{\mu 3})$ decay is also well suited to precision studies of other kaon decay modes. The

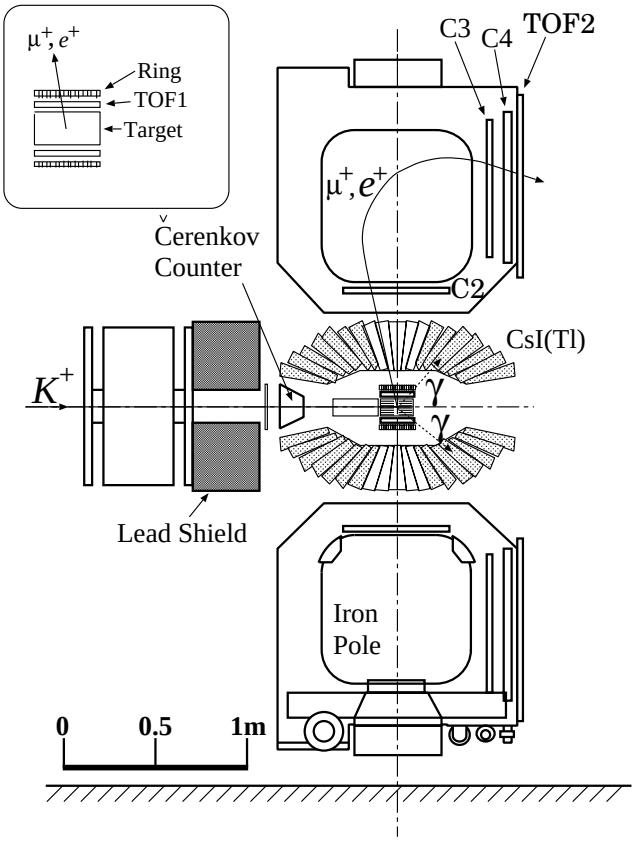

Fig. 25. Cross sectional side view of the detector, not showing the μ polarimeter which is located to the immediate right of TOF2. Assembly detail of the central region is shown in the inset.

detector, shown in Fig. 25, consists of an active scintillating-fibre target which serves as a kaon stopper and vertex detector, a CsI(Tl) calorimeter system which detects photons including π^0 decay, and a superconducting toroidal magnet spectrometer system to analyze and select μ^+'s, e^+'s, and π^+'s. A muon polarimeter system, not shown in Fig. 25, is located at the quasi-focal planes of the toroidal magnet gaps. The complete kinematics from stopped K-decay can be reconstructed from the charged track obtained in the target, ring scintillators and spectrometer tracking chambers, and from photons and π^0's in the photon detector array.

The T-violation search has been described in previous Annual Reports and the final data-taking was completed in 2000. During 2001 analysis effort was directed at the total data set taken since 1996. About two thirds of the data, through 1998, has yielded a result consistent with the standard model expectation of no T-violation. However, the inclusion of the data from the later runs has not been completed since they were taken under sufficiently different conditions that several systematic effects have required additional study.

Analysis of $K_{\ell 3}$ decays, where $\ell = \mu$ or e, was carried out in 2001. A reanalysis [Levchenko *et al.*, Proc. 3rd Int. Conf. on Nonaccelerator New Physics (NANPino 01), Dubna, June 19–23, 2001, hep-ex/0111048] of our K_{e3} decay data was carried out in order to attempt to reduce the errors further and thus improve the test for non-standard model scalar and tensor components in the electroweak form factors.

The most general Lorentz invariant form of the matrix element of K_{e3} decay can be written as

$$\begin{aligned} M \quad \propto \quad & f_+(q^2)(P_K + P_{\pi^0})^\lambda \bar{u}_e \gamma_\lambda (1-\gamma_5) u_\nu \\ & + f_-(q^2) m_l \bar{u}_e (1-\gamma_5) u_\nu + 2 m_K f_S \bar{u}_e (1-\gamma_5) u_\nu \\ & + (2 f_T / m_K)(P_K)^\lambda (P_{\pi^0})^\mu \bar{u}_e \sigma_{\lambda\mu} (1-\gamma_5) u_\nu, \end{aligned}$$

where $f_\pm(q^2)$, f_S and f_T are the vector, scalar and tensor form factors, P_K and P_π are four-momenta of the K^+ and π^0. The vector form factors $f_\pm(q^2)$ are assumed to be linearly dependent on the momentum transfer squared $q^2 = (P_K - P_\pi)^2$ and they can be represented by the equation $f_\pm(q^2) = f_\pm(0)(1 \pm \lambda_\pm(q^2/m^2_{\pi^0}))$. Because of the small mass of the positron, the part of the matrix element that depends on $f_-(q^2)$ is negligible and there are just three free parameters of the theory: λ_+, f_S and f_T. Within the standard model (SM), due to W-boson exchange, no terms other than those of a pure vector nature are expected. A possible contribution to f_S and f_T from electroweak radiative corrections is negligibly small and, therefore, non-zero values of f_S and f_T would signal new physics beyond the SM. Our first result [Shimizu *et al.*, Phys. Lett. **B495**, 33 (2000)] was unable to confirm previously reported non-zero values.

Compared to the first analysis, improvements in reconstruction of the charged particle track were made. In the new analysis, information about the kaon stopping position from the target (x, y) and ring counter (z) was included in the momentum reconstruction routine. The reconstruction of the π^0 kinematics was also improved by using tighter time windows in the CsI and improved calibration. The Monte Carlo routines more accurately described the kaon stopping distribution in the target and the electromagnetic shower leakage effects in the CsI. This allowed us to use all CsI crystals for reconstruction of the π^0, resulting in approximately a factor of four increase in acceptance.

Within the standard model the only parameter to be obtained is λ_+. It can be extracted in a model-independent way from the q^2 dependence of f_+. For extraction of all three parameters λ_+, f_S and f_T, the Dalitz distribution fit was performed using the P_{e^+}, $\theta_{\pi^0 e^+}$ variables. The angle between the pion and positron, $\theta_{\pi^0 e^+}$, was preferred instead of pion energy E_{π^0} in order to reduce a systematic error related to the energy leakage in the electromagnetic calorimeter. The values obtained for λ_+, and the scalar and tensor form factors are

$$\begin{aligned} \lambda_+ &= 0.0278 \pm 0.0017(\text{stat}) \pm 0.0015(\text{syst}) \\ f_S &= 0.0040 \pm 0.0160(\text{stat}) \pm 0.0067(\text{syst}) \\ f_T &= 0.019 \pm 0.080(\text{stat}) \pm 0.038(\text{syst}) \,. \end{aligned}$$

The statistical errors have been improved by a factor of 1.5 and systematic errors for λ_+, f_S and f_T were reduced by the factors 2.0, 2.1 and 2.4, respectively, compared to our previous result. This result is in agreement with the standard model prediction and there is no evidence for a deviation from zero for the values of scalar and tensor form factors.

In another analysis [Horie *et al.*, Phys. Lett. **B513**, 311 (2001)] the $K^+ \to \pi^0 \mu^+ \nu$ ($K_{\mu 3}$) events, which were collected simultaneously, were analyzed to determine the ratio of the $K_{\mu 3}$ and K_{e3} decay widths $\Gamma(K_{\mu 3})/\Gamma(K_{e3})$.

Assuming that only the $V - A$ interaction contributes to the $K_{\ell 3}$ decay, the decay amplitude can be described by the two dimensionless form factors $f_+(q^2)$ and $f_0(q^2)$, defined above, which are functions of the momentum transferred to the leptons $q^2 = (P_K - P_{\pi^0})^2$ where P_K and P_{π^0} are the four momenta of the K^+ and π^0, respectively. Assuming $\mu - e$ universality, the form factors for $K_{\mu 3}$ and K_{e3} decays are identical and $\Gamma(K_{\mu 3})/\Gamma(K_{e3})$ can be written as,

$$\Gamma(K_{\mu 3})/\Gamma(K_{e3}) = 0.6457 - 0.1531\lambda_+ + 1.5646\lambda_0 + \text{H.O.}$$

If the λ_+ value derived from the K_{e3} analysis is assumed, the λ_0 parameter can be obtained.

Data were taken at two spectrometer fields, 0.65 and 0.90 T, in order to study systematic effects. In the analysis $K_{\mu 3}$ and K_{e3} events were selected by time-of-flight of μ^+'s and e^+'s through the spectrometer, and the π^0's were identified from exactly two photon clusters in the CsI calorimeter.

In order to obtain the detector acceptance and estimate the background fraction, a Monte Carlo simulation was carried out for both the charged particle measurement in the spectrometer and the π^0 measurement in the CsI(Tl) detector. The initial Dalitz distributions were generated with the values of $\lambda_+ = 0.0278$ and the current world average $\lambda_0 = 0.006$, while the Dalitz distribution of K_{e3} decay is insensitive to the λ_0 parameter. The simulation data were analyzed in the same manner as the experimental sample.

The results obtained in this work are:

$$\begin{aligned} \Gamma(K_{\mu 3})/\Gamma(K_{e3}) &= 0.671 \pm 0.007(\text{stat}) \pm 0.008(\text{syst}), \\ \lambda_0 &= 0.019 \pm 0.005(\text{stat}) \pm 0.004(\text{syst}). \end{aligned}$$

The value of λ_0 obtained is consistent with that from $K_{\mu 3}$ Dalitz plot analyses [Whitman *et al.*, Phys. Rev.

D21, 652 (1980); Artemov *et al.*, Phys. of Atomic and Nuclei **60**, 2023 (1997)], which supports the validity of $\mu-e$ universality. If the assumption of $\mu-e$ universality is removed and values of λ_+^μ, λ_+^e, and λ_0 are taken from other work, then the result for $\Gamma(K_{\mu 3})/\Gamma(K_{e3})$ can be used to obtain the ratio of weak coupling constants $g_\mu f_+^\mu(0)/g_e f_+^e(0) = 0.971 \pm 0.019$, which is consistent with unity.

Finally, in October, 2001, the last beam time with the apparatus was used to study the radiative $K_{\pi 2}$ decay, $K^+ \rightarrow \pi^+\pi^0\gamma$. For this run, additional photon veto counters were added to detect photons escaping through the muon holes in the CsI(Tl) calorimeter. This decay channel is unique. The direct photon emission from the vertex is easy to observe because the internal bremsstrahlung contribution is suppressed by the $\Delta I = 1/2$ rule. This direct emission is dominated by the chiral anomaly of magnetic transitions and the decay amplitude can be analyzed in terms of chiral perturbation theory (ChPT). This measurement can potentially confirm and extend the recent result from BNL E787 [Adler *et al.*, Phys. Rev. Lett. **85**, 4856 (2000)] by virtue of its high kinematic resolution, and its capability to reach the lower π^+ energy region where the direct photon emission is more important. Analysis of these data is currently in progress.

TJNAF Experiment E00-006
Measurement of the flavour singlet form factors of the proton ($G\emptyset$)
(W.T.H. van Oers, Manitoba)

The structure of the nucleon at low energies in terms of the quark and gluon degrees of freedom is not well understood. The $G\emptyset$ experiment aims to measure two proton ground state matrix elements which are sensitive to point-like strange quarks and hence to the quark-antiquark sea in the proton. The matrix elements of interest are the elastic scattering vector weak neutral current charge and magnetic form factors, G_E^Z and G_M^Z, respectively. These can be extracted from a set of parity violating electron-proton scattering measurements. If one assumes a relationship between the proton and neutron structure in that the proton and neutron differ only by the interchange of up and down quarks, i.e., isospin symmetry, the strange quark (as well as the up and down quark) contribution to the charge and magnetic form factors of the nucleon can be determined. This would result from taking appropriate linear combinations of the weak neutral form factors and their electromagnetic counterparts.

Determinations of both the charge and magnetic strange quark form factors are of fundamental interest, as these would constitute the first direct evidence of the quark sea in low energy observables. It is the objective of the $G\emptyset$ experiment to determine these contributions to the proton form factors at the few per cent level. Observations at high energy suggest that the strange quarks carry about half as much momentum as the up and down quarks in the sea. It is important to determine both the role of the quark sea and the relevance of strange quarks at low energy where there are voids in understanding the theory of the strong interaction (quantum chromodynamics, QCD). Even if the strange quark contributions are found to be below the level of sensitivity of the experiment, upper limit determinations at this level are as valuable as non-zero results. The matrix elements G_E^Z and G_M^Z are also relevant to discussions of the Ellis-Jaffe sum rule and the pion-nucleon sigma term; there is uncertainty in both of these about the strange quark contributions. The $G\emptyset$ experiment will allow the determination of the strange contributions to the proton charge and magnetic form factors in a more straightforward manner.

In the $G\emptyset$ experiment parity violating longitudinal analyzing powers will be measured in electron-proton scattering in the range $0.1 \leq Q^2 \leq 1.0$ GeV^2 at both forward and backward angles. The longitudinal analyzing power is defined as

$$A_z = (1/P)\frac{[\sigma^+(\theta) - \sigma^-(\theta)]}{[\sigma^+(\theta) + \sigma^-(\theta)]}$$

where P is the polarization of the incident electron beam and the + and – superscripts indicate the helicity state. Making pairs of measurements at forward and backward angles will allow the separation of G_E^Z and G_M^Z. Predicted longitudinal analyzing powers range from about (–3 to 35) $\times$ 10^{-6}; it is planned to measure the longitudinal analyzing powers with statistical uncertainties of $\Delta A/A = 5\%$ and systematic uncertainties related to helicity correlated effects of $\Delta A/A \leq 2.5 \times 10^{-7}$. In the first phase of the experiment longitudinal analyzing powers will be measured concurrently at seven values of the momentum transfer in the range $0.1 \leq Q^2 \leq 1.0$ GeV^2. It now appears highly probable that by the time of data-taking for the $G\emptyset$ experiment (starting in 2002) higher beam polarizations (∼70%) will be available at the reduced beam pulse frequency of 31 MHz, decreasing considerably the original estimate of 700 hours for the first phase of the experiment. However, it must be realized that the length of the experiment is in part governed by making rather elaborate control measurements to determine the corrections that have to be made to the measured asymmetries and to assess systematic errors. In the second phase of the experiment each subsequent backward angle analyzing power measurement would require from one half to one month of running time. The results of the SAMPLE experiment at the MIT-Bates Laboratory have shown the importance of mea-

suring the axial form factor corrections, since these appear to be quite different from the theoretical predictions. Therefore, companion measurements of quasi-elastic scattering from deuterium will also be made at the backward angles. With these measurements, the effective axial current of the nucleon will also be determined. This current includes effects from the effective axial coupling of the photon to the nucleon or anapole moment, which are relevant also in other processes, e.g., parity violating Moller scattering and atomic parity violation.

The $G\emptyset$ collaboration

The $G\emptyset$ experiment will be carried out in Hall C at TJNAF by a collaboration of scientists from Canada, France, Georgia, and the United States, with funding provided through NSERC (Canada), IN2P3 (France), and DOE/NSF (US).

Canadian contributions

The Canadian members of the $G\emptyset$ collaboration, based at the universities of Manitoba and Northern British Columbia, and TRIUMF, have been asked to:

(i) develop and produce specialized photomultiplier tube bases for the main detector arrays;
(ii) design, build, and commission an automated magnetic field measuring apparatus complete with its own data acquisition system;
(iii) prototype and produce the cryostat exit detector arrays for the backward angle measurements;
(iv) prototype and produce the aerogel Čerenkov arrays for background rejection in the backward angle measurements;
(v) coordinate the implementation of TJNAF built beam monitors and control apparatus with TRIUMF built parity type electronics;
(vi) provide design and implementation support for the liquid hydrogen target slow controls system;
(vii) manage the coordination and scheduling of resources for $G\emptyset$ engineering runs at TJNAF.

Considerable progress has been made in the design and production of the subsystems listed above, many of which are now operational.

The $G\emptyset$ main detector array

The heart of the $G\emptyset$ detection system is a spectrometer which consists of an eight-sector toroidal magnet with an array of scintillation detectors located at the focal surface of each sector (see Fig. 26). Since data will not be acquired in event-by-event mode in this experiment, and since the scintillator arrays are the only detectors to measure the scattered particles in the forward angle mode, the performance of these focal-plane detectors (FPD) is of critical importance. The timing and pulse shape characteristics of this system must be

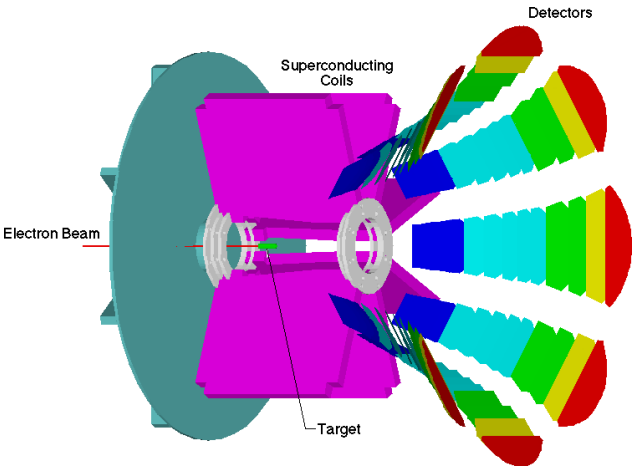

Fig. 26. View of the $G\emptyset$ superconducting toroidal spectrometer with one sector and the housing removed.

fine-tuned at the hardware level as it will not be possible to reconstruct individual events. Furthermore, the rates associated with many of the FPD elements will be quite high (1 MHz) and the photon yield(s) will have a large dynamic range. As such, special demands will be made on the photomultiplier tubes (PMT) and especially on their associated divider/base circuit. Work on the design, development, and production of the $G\emptyset$ bases began at TRIUMF in 1997. Several iterations of prototype high-rates bases were constructed and tested in late 1997 and early 1998. In the summer of 1998, 12 final prototype bases were constructed and delivered to TJNAF for tests with the first set of prototype FPDs, and fabrication of the production bases began. With the help of summer students (funded partly through the TRIUMF Summer Students program and partly through the $G\emptyset$ NSERC grant), the fabrication of the electrical components for all of the production bases was completed in 1998. The design of the mechanical housing for the PMT-base subsystem depended on the final design of the FPD support structure and, after much effort resolving subsystem integration issues, the final design for the PMT-base housing assembly was completed in late 1998. The fabrication and assembly of the mechanical housings and integration of the electrical components was completed over the summer of 1999 (again with the help of summer students at TRIUMF). Final testing of the completed bases was carried out in late fall, 1999, and shipment of all the bases (300 units) to TJNAF occurred at the end of calendar year 1999. Integration of this subsystem with the FPD arrays and the DAQ electronics was completed at TJNAF in 2000 and 2001 during the final assembly of the FPD system. Presently, all of the FPDs are fully instrumented and undergoing tests of the detector chain (scintillator/PMT-base/electronics/DAQ/analysis) in Hall C using cosmics and beam background.

Magnetic verification of the $G\emptyset$ spectrometer

An automated field measuring apparatus is being used to provide a magnetic verification of the $G\emptyset$ superconducting toroid by determining the locations of a pre-specified set of magnetic reference points. These reference points correspond to the zero-crossing locations of specific field components at selected points of symmetry around the toroidal magnet. This measurement is carried out by scanning a predefined set of contour lines, and determining where specific field components reverse sign. The system must be capable of providing a position determination of $\pm$ 0.2 mm and a field determination of $\pm$ 0.2 G. Considerable effort has gone into the design, construction and commissioning of this magnetic field measuring apparatus or magnetic verification device at TRIUMF, the University of Manitoba and UNBC. The device consists of a programmable gantry with full 3D motion anywhere within a 4 m $\times$ 4 m $\times$ 2 m volume, and a set of high precision Hall probes mounted at the end of a probe boom on the gantry (see Fig. 27). Procurement of parts commenced in early 2000, and final assembly and testing began in late spring 2000 at TRIUMF. The magnetic verification device was completed in midsummer, 2000 and transported to the University of Illinois to carry out the magnet measurements. Over the past year, much effort has gone into commissioning this device and upgrading the motion control and data acquisition software. In the spring of 2001, a series of measurements were carried out with the magnet energized at low currents. The magnetic verification device yielded remarkably consistent results and indicated that the final measurements, with the superconducting magnet at high current, should be straightforward. After many months of effort to cool the magnet coils, the $G\emptyset$ spectrometer made the transition to superconducting mode in late 2001 (December). At this point, the magnet was energized at high currents and two complete sets of magnetic field verification scans were carried out. These data are presently being analyzed and preliminary results will be available shortly. Shown in Fig. 28 is the magnetic verification device and the $G\emptyset$ superconducting spectrometer. Although this magnetic verification device was designed, tested, and built by the Canadian subgroup at TRIUMF and the universities of Manitoba and Northern B.C., it should be noted that funding for hardware components of this subsystem has been provided via NSF funding for

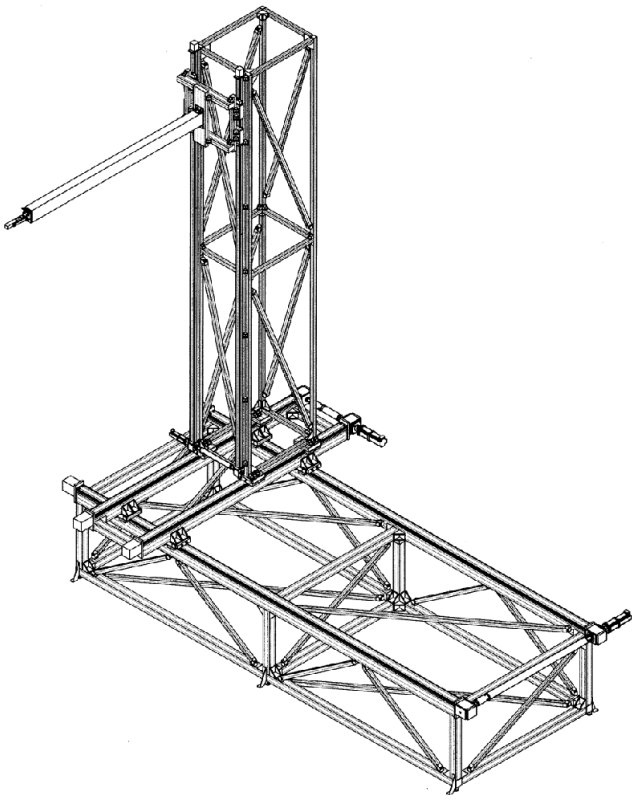

Fig. 27. Layout of the magnetic verification device, which consists of a programmable gantry (capable of full 3D motion anywhere within a 4 m $\times$ 4 m $\times$ 2 m volume) with a set of high precision Hall probes, temperature, inclination, and photo sensors mounted at the end of a probe boom on the gantry.

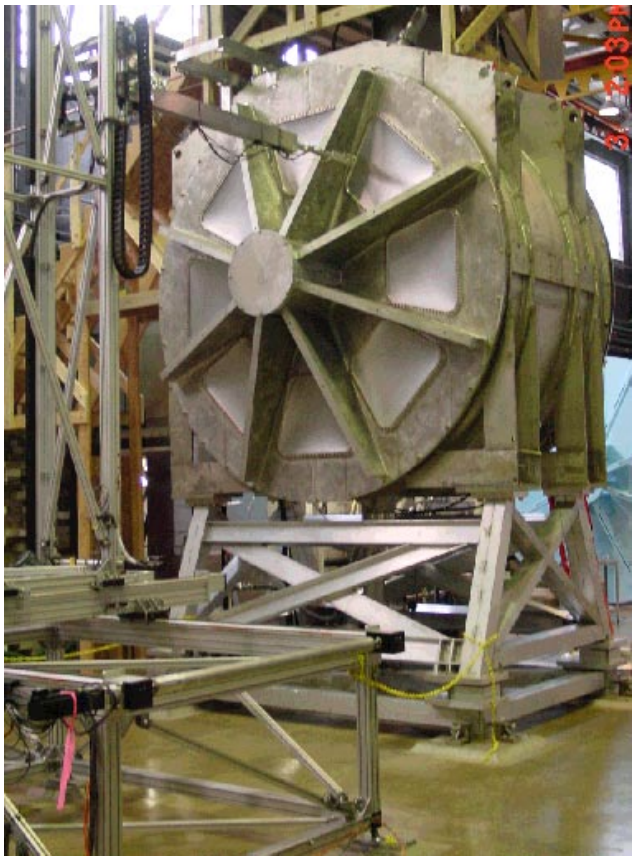

Fig. 28. The magnetic verification apparatus and $G\emptyset$ superconducting magnet at UIUC.

$G\emptyset$ through the University of Illinois. Infrastructure support, however, has been provided by TRIUMF and the Universities of Manitoba and Northern B.C.

The cryostat exit detector array

For the backward angle measurements during the second phase of the $G\emptyset$ experiment, the addition of a second array of scintillation detectors, located near the spectrometer cryostat exit windows, will be required in order to discriminate the elastically from the inelastically scattered electrons. The geometry of these cryostat exit detector (CED) arrays (see Fig. 29) has been studied in detail and a reference design was completed in the spring of 1999. With the resident expertise at TRIUMF in producing high quality scintillation detectors and lightguides, the Canadian subgroup was asked to play the main role in the prototyping and production of the CEDs. A set of prototypes was built at TRIUMF and delivered to Louisiana Tech University for further studies in early summer, 1999. Results from these studies indicate that the reference design and the prototype detectors will meet the specification requirements for the CED arrays. Production of a full set of dummy CED prototypes was then completed at TRIUMF in 2000, to aid in the design of the CED scintillator support structure. After finalizing the CED design, fabrication of the production versions of the CED arrays started at TRIUMF in late 2000. In fall 2001, the full 8 sets of CED scintillators were completed and delivered to TJNAF. Presently, fabrication of the helical-bending and transition lightguides for the CEDs is under way at TRIUMF, and a first set should be available for final assembly tests in spring, 2002. The CEDs will make use of the same photomultiplier tubes and specialized TRIUMF/$G\emptyset$ bases as the FPDs.

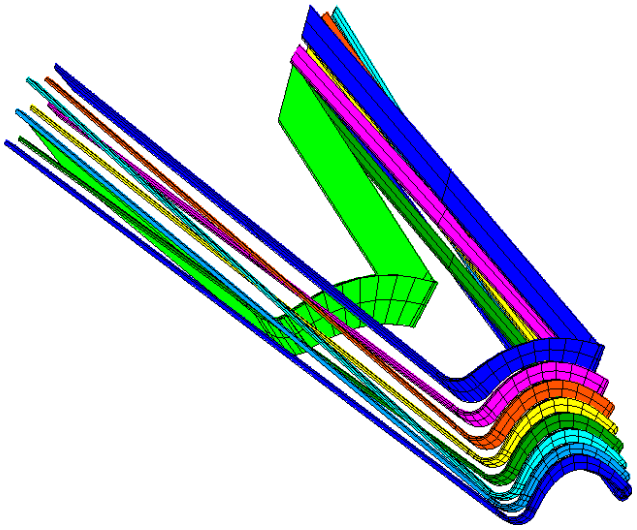

Fig. 29. Geometry of the cryostat exit detector (CED) array for a single octant.

Aerogel Čerenkov array

Monte Carlo simulation results have shown that backgrounds from negative pions will be problematic for the second phase backward angle measurements. Recent efforts of the $G\emptyset$ Simulation subgroup have focused on characterizing this π^- background and providing options regarding the design of an additional set of detectors to reject the background pions. The $G\emptyset$ Canadian and French subgroups have been asked to undertake the construction of this crucial set of additional detectors, which will be made up of arrays of aerogel Čerenkov counters. Over the past year, much effort has gone into the design of this detector array and its support structure. A conceptual design (see Fig. 30) has been evolved into a first prototype (see Fig. 31) at TRIUMF and has undergone tests with both cosmics and beam. In December, 2001, a test run was conducted in the M11 area. Two Čerenkov detectors, one built at TRIUMF and one built at Caltech, were placed in the M11 beam along with three scintillators to establish a trigger on the incident beam particles. The two Čerenkov detector light boxes were similar in size but somewhat different in shape and total light diffusion volume. Data were collected at 120, 200, 300, 350, and 400 MeV/c; the maximum momentum of the $G\emptyset$ π^-'s is 400 MeV/c. At these momenta the electrons have a high velocity and should always produce Čerenkov light while the pions have

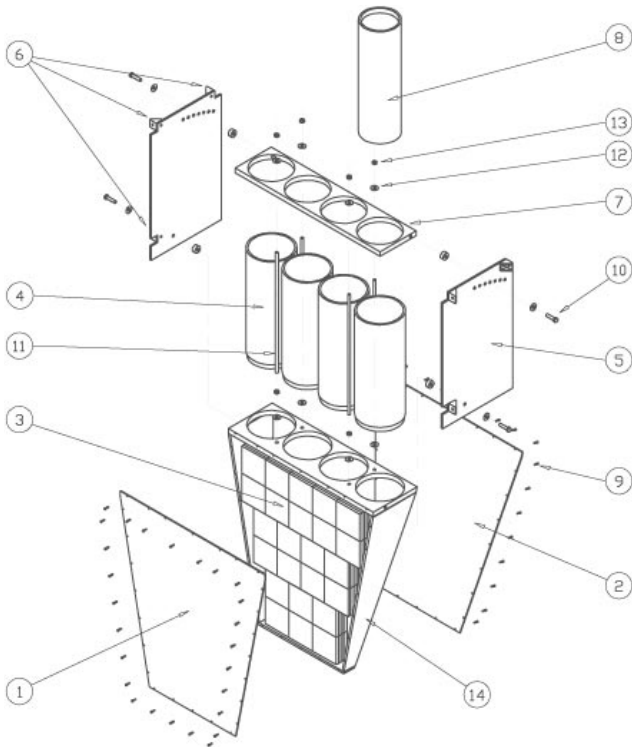

Fig. 30. Conceptual layout of the aerogel Čerenkov veto detector for a single octant.

Fig. 31. Prototype aerogel Čerenkov detector at TRIUMF.

a velocity below the Čerenkov threshold. The light yield and timing spread were studied as a function of beam momenta, position and angle of incidence. Preliminary results indicate some differences between the boxes and variation in the light yield with both position and angle. These results are presently being studied with Monte Carlo techniques, and further testing with cosmics is under way. Depending on the results of these studies, a second iteration prototype may be used in further in-beam tests in M11, planned for summer, 2002. Shown in Fig. 32 is a conceptual illustration of the $G\emptyset$ backward angle configuration with the superconducting magnet, the 3 detector arrays (FPD, CED, Čerenkov) in each of the 8 sectors, and their respective support structures.

Beam monitors and parity electronics

Five sets of XYQ monitors will be required in order to measure the beam current and trajectory at several critical locations. A beam current sensitivity of $\pm\, 4 \times 10^{-5}$ measured in a 33 ms integration-time sample will be required to monitor and correct for possible helicity correlated intensity modulations. For the beam position monitors (BPMs), a spatial resolution of better than 25 μm at an integration time of 33 ms will be required. Some of the beam current and position

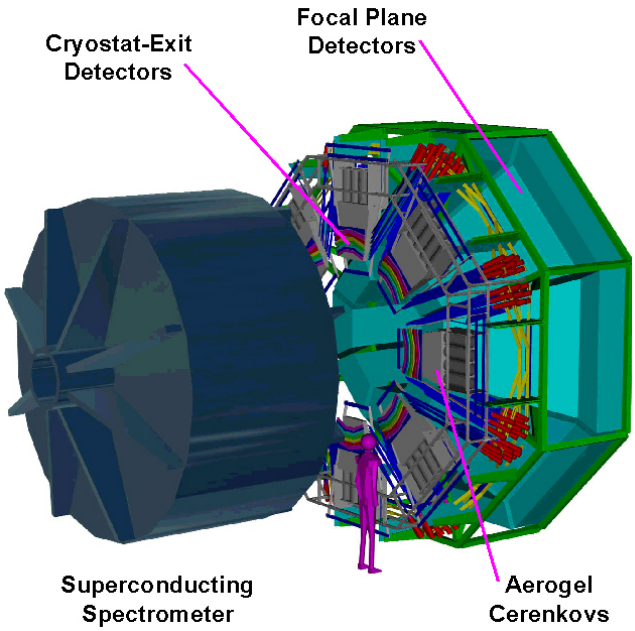

Fig. 32. Conceptual layout of the $G\emptyset$ backward angle configuration.

monitors were tested during an engineering run in July 1997 at TJNAF. The run was organized by members of the $G\emptyset$ Canadian subgroup and personnel from TJNAF (Hall C), with much of the parity type electronics provided by the Canadian subgroup. Helicity correlated properties of the TJNAF polarized electron beam and noise characteristics of some of the beam monitors were successfully measured. Analysis of the data indicates that the beam current and position monitors will meet the specification requirements listed above. Further test beam time is planned for the future. To read out the analogue signals from the beam current and position monitors, and to provide feedback control signals, specialized parity type electronics is required for the $G\emptyset$ experiment. Much of this electronics, such as precision analogue subtractors/dividers and precision voltage-to-frequency converters, has already been designed and used by members of the Canadian subgroup in their parity experiments at TRIUMF. Modifications, driven by $G\emptyset$ requirements, were made to some of these modules and they were operated successfully at the July, 1997 engineering run at TJNAF, as mentioned above. Since that time, several voltage-to-frequency converters of the TRIUMF/parity variety have been requested by TJNAF for the $G\emptyset$ experiment. Construction of these 32-channel precision V-to-Fs was completed at TRIUMF and delivery made to TJNAF in early 1998. With the successful implementation of these first sets of converters, a second set of V-to-F modules was requested by TJNAF in summer, 1999. This second set of V-to-F modules was again constructed at TRIUMF and delivered to TJNAF in

fall, 1999. A third set of V-to-F modules was requested and delivered to TJNAF in 2000. It is anticipated that several more sets of V-to-F modules, as well as other specialized parity type electronics modules, will be required by the $G\emptyset$ collaboration over the next few years, as the experiment moves into the commissioning and data-taking phase.

Slow controls for cryogenic target system

The $G\emptyset$ experiment will use a 20 cm long liquid hydrogen (LH_2) target connected to a cryogenic loop to recirculate and cool the liquid. This target will operate at 20 K and 25 psia, and the heat deposited by the 40 μA electron beam will be carried away from the hydrogen by a compressed He gas heat exchanger. The main components of the target system are a pump for circulating the target fluid in a closed cryogenic loop, a heat exchanger, the target cell, and a manifold to direct the fluid flow down the centre of the target cell. A gas handling system is employed to provide gas to the target, the He coolant to the heat exchanger, and to evacuate the region surrounding the target. The state of the target (temperatures, pressures, position, etc.) and the gas handling system (valve settings) is monitored/controlled by what is called the slow controls system. This system sounds alarms when operating conditions become improper, monitors beam current and maintains a constant heat load on the target. The control system also records the target state at regular intervals to log files. The Canadian subgroup has been providing design and implementation support for the liquid hydrogen target slow controls system. Specifically, the responsibilities include: (a) participation in MEDM monitoring and control screens design; (b) installation and integration into the system of the Joule-Thompson valve controller to control the flow of the He coolant; (c) testing of target and He coolant temperature sensors; (d) participation in the pressure transducer calibration and target motion testing/calibration; and (e) configuration and management of the channel archiver software which logs and plots the target data. Members of the Canadian subgroup have taken part in the test cooldowns of the target and are also involved in the design of the $G\emptyset$ main screen software which displays the experiment and system status.

***G*$\emptyset$ engineering runs**

Several engineering runs have been carried out by the $G\emptyset$ collaboration to study (a) the helicity correlated properties of the TJNAF polarized electron beam and the noise characteristics of the Hall C beam line monitors (July, 1997); and (b) the neutron background and energy spectrum in the vicinity of the $G\emptyset$ detector system (December, 1999). Both these efforts were coordinated by members of the Canadian subgroup and personnel from TJNAF (Hall C) with much of the equipment provided by the Canadian subgroup. Presently, as construction of the first-phase forward-angle mode of the $G\emptyset$ experiment nears completion, the individually complex systems comprising the experiment must be integrated into one overall system. To accomplish this, the collaboration will undertake a number of engineering runs to test the functionality of these systems and identify deficiencies. These engineering runs will ultimately test the interaction of the complete system, which includes the data acquisition system, detectors, analysis software, and magnet and target controls. Members of the Canadian subgroup, together with the University of New Mexico subgroup, have planned and detailed the requirements and benchmarks of the engineering runs. Coordination and scheduling of resources for the engineering runs is being managed by members of the $G\emptyset$ Canadian subgroup. The goals of the engineering runs are: commission and test the individual systems; schedule and verify mechanical assembly of sub-assemblies; integrate the systems to establish the fundamental detector and DAQ operation(s); identify and correct deficiencies and system conflicts; test and verify that the composite system is capable of parity violation asymmetry measurements.

Canadian subgroup of the $G\emptyset$ collaboration: J. Birchall, J. Chiang, B. Chow, W.R. Falk, M. Hasselfeld, A. Horning, L. Lee, S.A. Page, W.D. Ramsay, A. Rauf, G. Rutledge, M. Steeds, W.T.H. van Oers (Manitoba); E. Korkmaz, T. Porcelli (Northern British Columbia); C.A. Davis (TRIUMF).